Geochemistry 79 (2019) 125525

Contents lists available at ScienceDirect

Geochemistry

journal homepage: www.elsevier.com/locate/chemer

The Renchen L5-6 chondrite breccia – The first confirmed meteorite fall from Baden-Württemberg (Germany)

Addi Bischoff[a,*], Jean-Alix Barrat[b], Jasper Berndt[c], Jiri Borovicka[d], Christoph Burkhardt[a], Henner Busemann[e], Janina Hakenmüller[f], Dieter Heinlein[g], Jasmine Hertzog[h,i], Jozef Kaiser[j], Colin Maden[e], Matthias M.M. Meier[e,k], Précillia Morino[e], Andreas Pack[l], Markus Patzek[a], Maximilian P. Reitze[a], Miriam Rüfenacht[e], Philippe Schmitt-Kopplin[h,i], Maria Schönbächler[e], Pavel Spurný[d], Iris Weber[a], Karl Wimmer[m], Tomas Zikmund[j]

[a] Institut für Planetologie, Westfälische Wilhelms-Universität Münster, Wilhelm-Klemm Str. 10, D-48149, Münster, Germany
[b] Université de Bretagne Occidentale, Institut Universitaire Européen de la Mer, Place Nicolas Copernic, F-29280, Plouzané Cedex, France
[c] Institut für Mineralogie, Westfälische Wilhelms-Universität Münster, Corrensstr. 24, D-48149, Münster, Germany
[d] Astronomical Institute of the Czech Academy of Sciences, Fričova 298, CZ-25165, Ondřejov, Czech Republic
[e] Institute for Geochemistry and Petetrology, ETH Zurich, Clausiusstraße 25, CH-8092, Zurich, Switzerland
[f] Max-Planck-Institut für Kernphysik, Saupfercheckweg 1, D-69117, Heidelberg, Germany
[g] German Fireball Network, Lilienstraße 3, D-86156, Augsburg, Germany
[h] Helmholtz-Zentrum, München, German Research Center for Environmental Health, Analytical BioGeoChemistry, Ingolstädter Landstraße 1, D-85764, Neuherberg, Germany
[i] Chair of Analytical Food Chemistry, Technische Universität München, D-85354, Freising-Weihenstephan, Germany
[j] CEITEC - Central European Institute of Technology, Brno University of Technology, Purkynova 123, CZ-61200, Brno, Czech Republic
[k] Naturmuseum St. Gallen, Rorschacher Strasse 263, CH-9016, St. Gallen, Switzerland
[l] Universität Göttingen, Geowissenschaftliches Zentrum, Goldschmidtstr. 1, D-37077, Göttingen, Germany
[m] RiesKraterMuseum, Eugene-Shoemaker-Platz 1, D-86720, Nördlingen, Germany

ARTICLE INFO

Handling Editor: Falko Langenhorst

Keywords:
Ordinary chondrite
Chondrite breccia
L chondrite
Meteorite fall

ABSTRACT

On July 10, 2018 at 21:29 UT extended areas of South-Western Germany were illuminated by a very bright bolide. This fireball was recorded by instruments of the European Fireball Network (EN). The records enabled complex and precise description of this event including the prediction of the impact area. So far six meteorites totaling about 1.23 kg have been found in the predicted location for a given mass during dedicated searches. The first piece of about 12 g was recovered on July 24 close to the village of Renchen (Baden-Württemberg) followed by the largest fragment of 955 g on July 31 about five km north-west of Renchen.

Renchen is a moderately-shocked (S4) breccia consisting of abundant highly recrystallized rock fragments as well as impact melt rock clasts. The texture, the large grain size of plagioclase, and the homogeneous compositions of olivine (~Fa_{26}) and pyroxene (~Fs_{22}) clearly indicate that Renchen is composed of metamorphosed rock fragments (L5–6). An L-group (and ordinary chondrite) heritage is consistent with the data on the model abundance of metal, the density, the magnetic susceptibility as well as on O-, Ti-, and Cr-isotope characteristics. Renchen does not contain solar wind implanted noble gases and is a fragmental breccia. An unusually large mm-sized merrillite-apatite aggregate shows trace element characteristics like other phosphates from ordinary chondrites.

Data on the bulk chemistry, IR-spectroscopy, cosmogenic nuclides, and organic components also indicate similarities to other metamorphosed L chondrites. Noble gas studies reveal that the meteorite has a cosmic ray exposure (CRE) age of 42 Ma and that most of the cosmogenic gases were produced in a meteoroid with a radius of at max. 20 cm based on the radionuclide ^{26}Al and 10–150 cm based on cosmogenic ^{22}Ne/^{21}Ne. K-Ar and U/Th-He gas retention ages are both in the range ~3.0–3.2 Ga. Both systems do not show evidence for a complete reset 470 Ma ago, and may instead have recorded the same resetting event 3.0 Ga ago.

* Corresponding author at: Institut für Planetologie, Westfälische Wilhelms-Universität Münster, Wilhelm-Klemm-Str. 10, D-48149, Münster, Germany.
E-mail address: bischoa@uni-muenster.de (A. Bischoff).

https://doi.org/10.1016/j.chemer.2019.07.007
Received 2 May 2019; Received in revised form 22 July 2019; Accepted 26 July 2019
0009-2819/ © 2019 The Authors. Published by Elsevier GmbH. This is an open access article under the CC BY-NC-ND license (http://creativecommons.org/licenses/BY-NC-ND/4.0/).

1. Introduction

On July 10, 2018, at 21:29:49-53 UT a -13.4 maximum absolute magnitude bolide was observed by many eyewitnesses mainly over South-Western Germany, Eastern France, Switzerland, and the Benelux countries. This spectacular fireball (known as EN100718 Renchen), which was for a short time even brighter than the light of the full Moon, was recorded photographically and photo-electrically by instruments of the Czech and German parts of the European Fireball Network (EN). Based on these instrumental data, precise results on atmospheric trajectory, heliocentric orbit, and fragmentation history were quickly determined. The luminous path of the bolide (having a steep trajectory) was 63 km long, for which the meteoroid required 4 s. The object entered the atmosphere with a speed of slightly less than 20 km/s, gradually decelerated, and fragmented. From the analysis at the Astronomical Institute of the Czech Academy of Sciences in Ondřejov (Czech Republic) it was quite clear that this event must have led to a multiple meteorite fall in the state of Baden-Württemberg (SW Germany) close to the river Rhine. The strewn field with the possible range of meteorite masses was immediately calculated (Fig. 1). The predicted impact area of meteorite fragments of all sizes mainly lies in the area of the town of Renchen. Smaller fragments originating from the main flare in 28 km height should be found in the eastern part of the predicted area with rising masses westwards. On the other hand, the heaviest pieces originating from the terminal point, which was about 10 km lower in the atmosphere and should have fallen within a narrow strip northwest of Renchen (Fig. 1). Shortly after the fall, the results were sent to one of the authors (D.H.) in Augsburg (Germany), member of the German Fireball Network. Search activities began July 15. Although the search conditions (e.g., high vegetation, high temperatures, and inaccessibility of some areas) were extremely difficult, already on July 24, a first meteorite fragment weighing 12 g was found (Table 1). The so far largest discovered piece (955 g) was found in a meadow, where it was only minimally sunk into the soil. As a result of the search activities all six meteorite fragments detected so far have been found in the predicted location for a given mass (Table 1; Fig. 1).

In this paper the mineralogical, chemical and isotopic characteristics of this new meteorite will be presented including data on organics, short-lived cosmogenic radioisotopes, and noble gases. The meteorite “Renchen” has been accepted by the Nomenclature Committee (The Meteoritical Bulletin, 2019).

After the meteorite falls of Braunschweig (L6; Bartoschewitz et al., 2017), Žd'ár nad Sázavou (L3; Spurný, 2016; Spurný et al., 2016), and Ejby (H5/6; Spurný et al., 2017a; Haack et al., 2019), Stubenberg (LL6; Ebert and Bischoff, 2016; Spurný et al., 2016; Bischoff et al., 2017a), Hradec Králové (LL5; 2016; The Meteoritical Bulletin), and Broek in Waterland (L6, 2017; The Meteoritical Bulletin) Renchen is the seventh recovered meteorite fall since 2013 impacting Earth in an area with a radius of < 500 km. On average, less than 10 meteorite falls/year are recovered globally (The Meteoritical Bulletin), and hence, this concentration of recorded falls in Central Europe is remarkable, which in part demonstrates the great success of the European Fireball Network in recording and calculating fireball events and possible meteorite strewn fields and ultimately finding the respective/associated meteorites.

2. Samples and a summary of methods

Until March 2019, six pieces with a total mass of 1227 g were recovered within the predicted fall area (Table 1; Fig. 1). Two of the meteorites (5 g and 6 g) have not reached the Earth's surface, since these pieces were caught by the hail protection net covering a fruit plantation (Fig. 2).

Different analytical methods were applied in order to reveal details on chemical, physical, and mineralogical features of the rock and to classify this meteorite. Here, a brief summary about the methods are given and further details are included in the “Supplementary Materials”. Several thin and thick sections of the Institut für Planetologie (PL18087, PL18088, PL18089, PL18090) of the Renchen chondrite were studied using optical and electron microscopy (Figs. 3–5). Scanning electron microscopic (SEM) studies were performed in Münster and Munich, while microprobe, as well as Raman spectroscopic investigations, were performed in Münster. X-ray microcomputed tomography (μCT) studies were performed at the Central European Institute of Technology, Brno University of Technology (CEITEC BUT). Metals, sulfides, silicates, and pores can easily be distinguished by this technique (Fig. S1). The trace element compositions

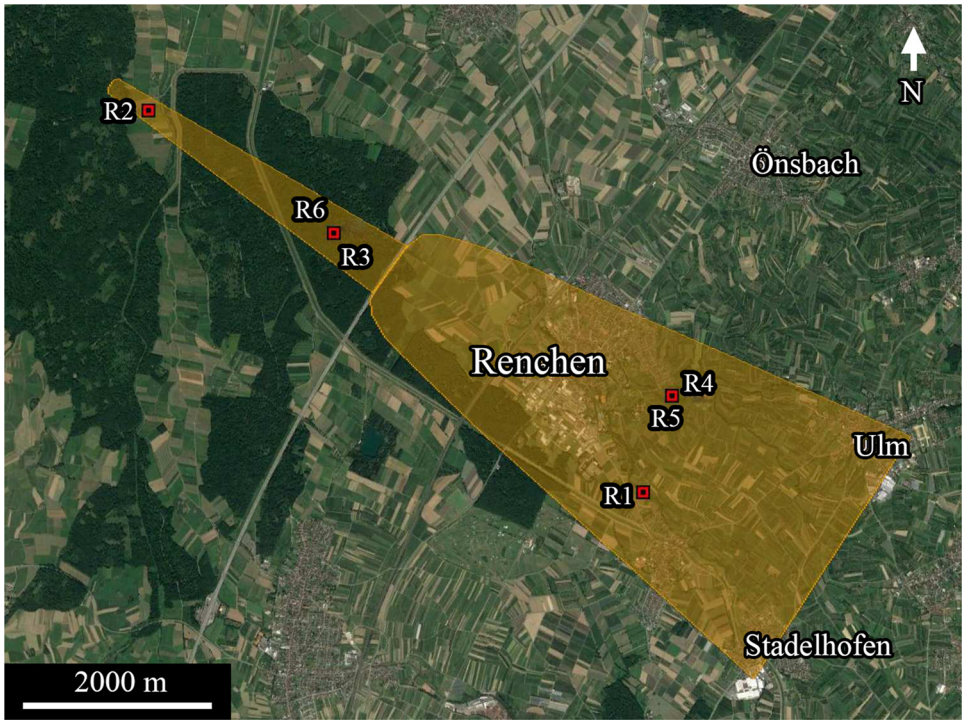


Fig. 1. Calculated strewn field near Renchen (Germany) with find locations of the six recovered individuals (R1 – R6). The north-western part of the strewn field is dominated by forest (dark green), where the samples R2, R3, and R6 were found. R2 was found in a meadow. Most other areas represent farmland or the city of Renchen. Source of base map: Google Earth.

Table 1
The Renchen meteorite finds (GPS coordinates of the locations referring to the WGS84 datum).

No.	Mass (g)	Date of find (yyyy-mm-dd)	Latitude (N)Longitude (E)	Characteristics of the meteorite piece; Finder of the specimen
R1	11.94	2018-07-24	48.574000° 8.019111°	Complete individual meteorite; Ralph Sporn + Martin Neuhofer
R2	955	2018-07-31	48.610222° 7.948167°	Individual meteorite with a broken face; Ralph Sporn + Martin Neuhofer
R3	20.59	2018-09-01	48.598608° 7.974818°	Several fragments; 17.89 g Lukasz Smula + Magda Skirzewska, 2.70 g Thomas Kurtz
R4	4.82	2018-09-30	48.583150° 8.023250°	Complete individual meteorite; Ralph Sporn + Martin Neuhofer
R5	6.29	2018-10-13	48.583050° 8.023300°	Complete individual meteorite; Martin Kappler
R6	228.2	2019-02-23	48.598690° 7.974810°	Individual meteorite with broken faces; Thomas Kurtz + Oliver Sachs
Total	1227		48° 35.3' 8° 00.0'	

of the Ca-phosphates were analyzed at the Institut für Mineralogie (WWU Münster) by a Finnigan Element 2 single collector ICP-MS coupled with Excimer laser ablation system using NIST-SRM 612 glass, basaltic BIR-1G (Jochum et al., 2005) and phosphatic STDP5 (Klemme et al., 2008) reference glasses as standards or reference materials.

A 283 mg whole-rock sample of Renchen was analyzed for major and trace element concentrations by inductively-coupled plasma atomic emission spectroscopy (ICP-AES) and inductively-coupled plasma sector field mass spectrometry (ICP-SFMS) following the procedure described by Barrat et al. (2012,2015,2016). For comparison a 206 mg sample of the weathered H4-5 chondrite Cloppenburg was analyzed.

Cosmogenic radionuclide concentrations were analyzed at the Max-Planck-Institut für Kernphysik in Heidelberg (Heusser et al., 2015) and bulk oxygen isotope compositions of two samples were obtained by means of laser fluorination with details on the technique and normalization reported in Pack et al. (2016).

Titanium and Cr isotope analyses on 30–50 mg samples of Renchen were performed using a ThermoScientific NeptunePlus multi-collector inductively coupled plasma mass spectrometer (MC-ICPMS) at the Institut für Planetologie (WWU Münster) and at the Institute for Geochemistry and Petrology (ETH Zurich). The analytical procedures followed previously established routines (Schönbächler et al., 2004; Williams, 2015; Zhang et al., 2011 for Ti; Trinquier et al., 2008a, b Steele and Schönbächler, 2016 for Cr) and are described in more detail in the "Supplementary Materials". Titanium isotope data were corrected for instrumental mass-bias by internally normalization to a $^{49}Ti/^{47}Ti$ ratio of 0.749766 (Niederer et al., 1981). For Cr, the $^{50}Cr/^{52}Cr$ ratio was used with a reference value of 0.051859 (Shields et al., 1966) The Cr isotope data is reported as the parts per ten thousand deviation from the Cr NIST SRM 979 standard.

Noble gases (all isotopes of He-Xe) were analysed in two interior samples (29.633 ± 0.0015 and 32.563 ± 0.0008 mg) at ETH Zurich with established routines detailed by Riebe et al. (2017). Samples were extracted by fusion at ~1700 °C, which was proven by repeat extractions at ~1750 °C to be complete. Blank corrections were negligible for He and Ne and ≤1.4% for $^{38,40}Ar$, ~8% for ^{36}Ar, ~30% for ^{84}Kr, ~5% for ^{132}Xe.

The infrared (IR) spectroscopic measurements were undertaken using a Bruker Vertex 70v at the IR/IS laboratory located at the Institut für Planetologie (Münster).

The Magnetic Susceptibility (MS) was measured with the handheld device SM-30 from ZH Instruments (www.zhinstruments.cz) and corrected for sample shape and mass. Two values at different orientations were taken for each of 4 individuals and of 16 pieces of the fragmented stone R3 of 11.9 g down to 0.18 g, one value for a set of tiny fragments with a total mass of 0.11 g; six values were obtained from the main mass of 955 g.

About 20 mg fresh fragments of the Renchen meteorite was first washed in LC/MS grade methanol prior destructive extraction with methanol in an agate mortar. The same extraction and analytical procedure using direct injection ultrahigh resolution mass spectrometry (UHRMS) was used as for the Stubenberg meteorite (Bischoff et al., 2017a) or originally for Murchison as described previously in Schmitt-Kopplin et al. (2010, 2012). Ultrahigh-resolution mass spectrometry enables us to obtain and evaluate the high number (several thousands) of distinct features in one analysis, which can be converted into elementary compositions of C, H, N, O, and S (Tziotis et al., 2011; Schmitt-Kopplin et al., 2012). To visualize such amounts of data, graphical presentations are required. Among them, the van Krevelen diagram is a well-established tool used in the field of complex mixtures of organic species such as heavy oils or kerogens, and terrestrial organic matter (Meckenstock et al., 2014; Hertkorn et al., 2015, 2016). As part of the study of soluble organic matter in meteorites, the thousands of CHNOS and CHOMg formulae (species) are plotted according to their atomic ratios (mostly O/C vs. H/C) with the size of the data points (bubbles) normalized to the mass spectrometric intensity of a given organic specie (molecule). The presentation of these data in the diagram is described as the "chemical space "or "compositional space" of the given sample.

3. Results

3.1. Fall circumstances and geographic details of find area

From the detailed light curve of the observed bolide taken by the hi-speed photometers, included in the automated cameras in the Czech part of the EN, it was certain that the initial meteoroid heavily fragmented in the last part of its luminous flight through the atmosphere (compare Spurný et al., 2007, 2017a,b). A calculation of the impact area was obtained by using precise trajectory data combined with the known wind conditions in the higher atmospheric layers. The resulting predicted strewn field, near the village of Renchen (~7400 residents, between Offenburg and Baden-Baden) in Baden-Württemberg has a complex shape (Fig. 1). However, the predicted area was convincingly confirmed by the positions and masses of the recovered meteorites, as described in Fig. 1. The north-western part of the strewn field at an elevation of about 200 m above sea level is dominated by forest including some meadows (at the very end of the strip), where the large sample R2 was found (Table 1; Fig. 1). Most other areas - especially in the south-east - represent farmland (Fig. 1).

3.2. Petrography and mineralogy

3.2.1. Description of hand specimens

All six recovered stones of the Renchen meteorite are shown in Fig. 2 and listed in Table 1. The first meteorite fragment R1 was found only two weeks after the fall during intensive search. Already after this short time interval the rock had been slightly affected by minor weathering as documented in places by the brownish taint on its

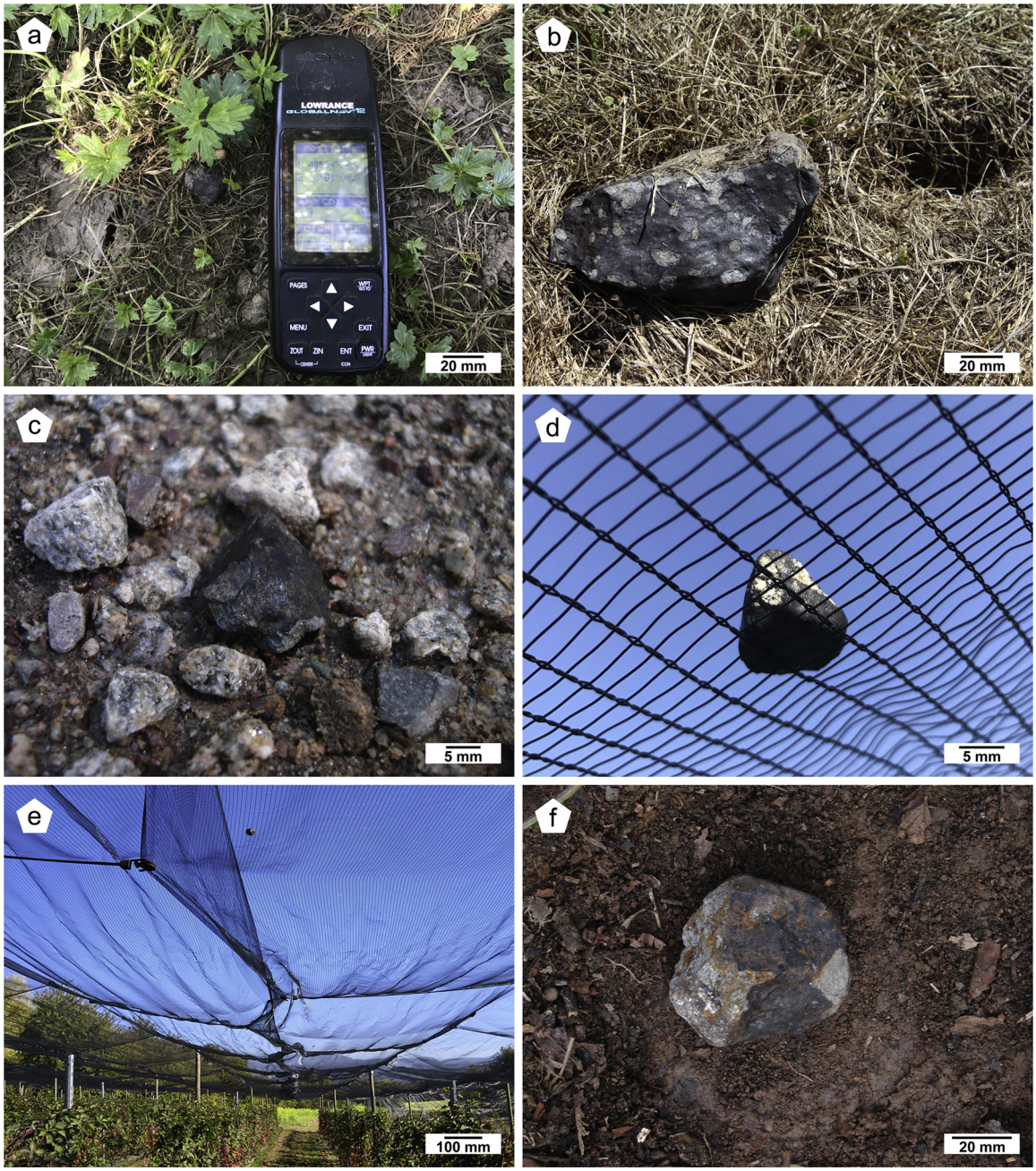


Fig. 2. In situ images of the six Renchen meteorites found between July 24, 2018 and February 23, 2019. (a) The complete individual meteorite R1 of 11.94 g was discovered on the ground of a cherry fruit plantation. (b) Main mass of Renchen R2 weighing 955 g in finding position on a withered field beneath the shallow impact hole. (c) This broken fragment R3A of 8.62 g is the largest part of 19 pieces, totaling 20.59 g, found scattered on a graveled forest path. (d) The small, complete meteorite piece R4 of 4.82 g did not reach the ground because it was caught by the hail protection net covering a raspberry/blackberry fruit plantation. (e) On top of the same netting also the individual meteorite R5 of 6.29 g was detected. (f) The second largest piece R6 weighing 228.2 g was found close to the location of the R3 fragments in the ditch of a forest track, buried under lots of broken branches.

surface. The large piece R2 of 955 g and also the meteorite individuals R1, R4, R5, and R6 have lost parts of the fusion crust. The fusion crust of R2 appears to have had variable thicknesses prior to impact on the ground (Fig. 2b). Similar observations were made on pieces of the Stubenberg meteorite (Bischoff et al., 2017a) and probably due to fragmentation events at different altitudes during transit through the atmosphere.

The inside of the broken fragment R3 is dominated by a greyish, silicate-rich component. Rare mm-sized fragments are visible and minor amounts of minerals with metallic lustre are recognizable throughout the rock. In places the chondritic texture is shadowy visible. Some thin shock veins are observed, which appear black on the surface of the fragments. Within some broken pieces mm-sized honey-yellow areas were detected (Fig. 4), which have been studied in detail (see below).

3.2.2. *Mineralogy – texture and compositions of phases*

The thin sections show that the rock is a breccia and consists of equilibrated and recrystallized lithologies (Figs. 3–5). All fragments show a recrystallized texture with some having a small number of chondrule relicts (Figs. 3c-f). Especially the outlines of former barred-olivine (BO) and radial pyroxene (RP) chondrules are still recognizable. One relict object is a compound BO chondrule with many siblings and another one is a macrochondrule (Figs. 3e,f; compare Weyrauch and Bischoff, 2012; Bischoff et al., 2017b). Olivine is by far the most

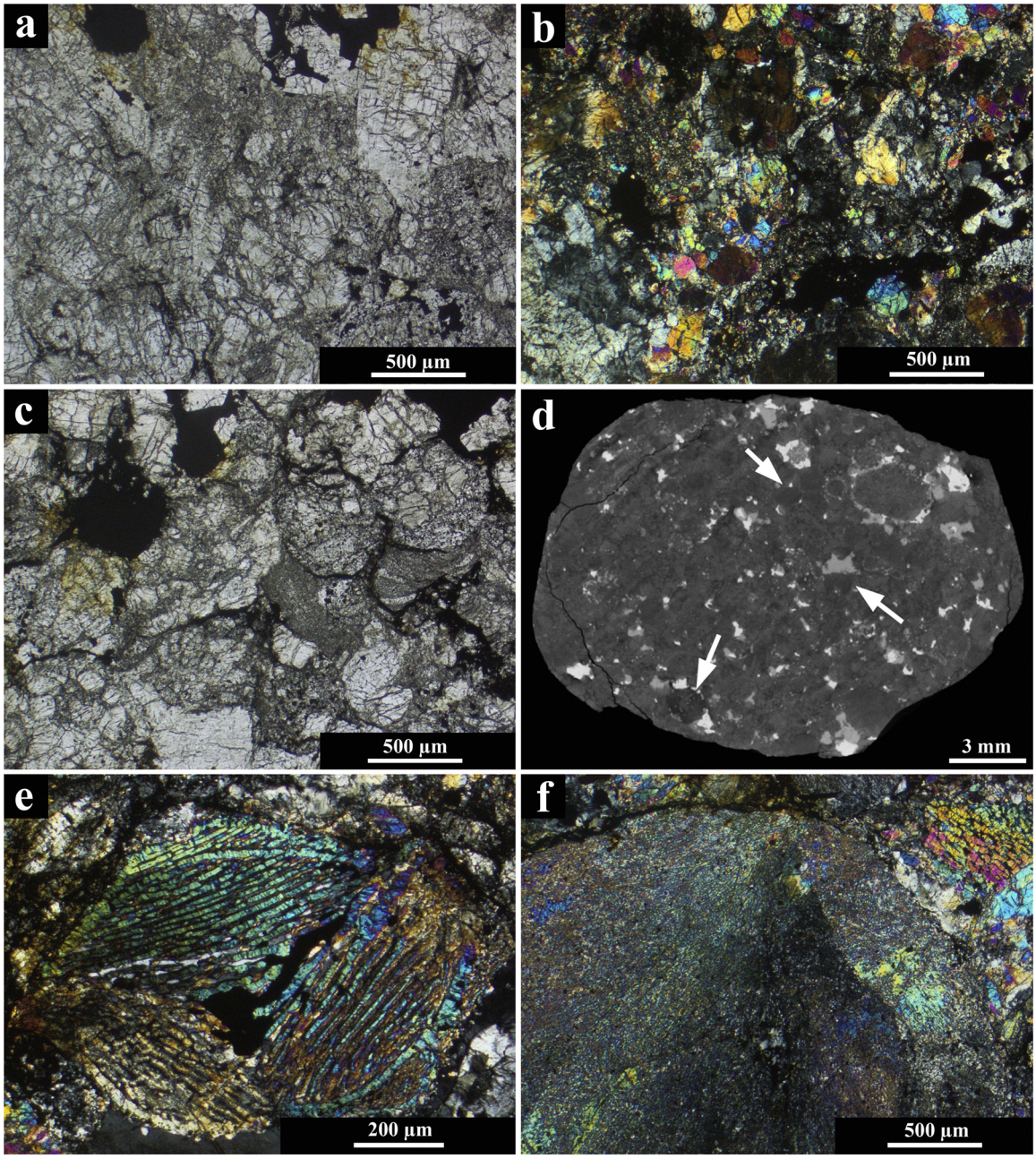


Fig. 3. (a,b) Characteristic images of a strongly recrystallized, type 6 area of Renchen having no obvious relict chondrules. (c) Areas of fragments with clearly-detectable relict chondrules (type 5). (d) CT-image of a slice from R1 showing the chondritic texture. Some objects appear to be quite dark (arrows) based on the low mean mass. (e) Relict compound barred-olivine (BO) chondrule. (f) Part of a ~4 mm-sized radial-olivine-pyroxene macrochondrule. Images in polarized light; crossed Nicols in (b), (e), and (f).

abundant phase and homogeneous in composition throughout all polished sections. The mean composition of 59 analyzed olivines is $Fa_{26.1 \pm 0.5}$ with a compositional range between 24.6 and 27.1 mol% Fa (Fig. 6; Table 2). The low-Ca pyroxenes and Ca-pyroxenes have compositions of $Fs_{21.9 \pm 0.3}Wo_{1.4 \pm 0.3}$ and $Fs_{7.6 \pm 0.7}Wo_{44.8 \pm 0.6}$, respectively (Table 2). The 21 analyzed low-Ca pyroxenes vary between 21.1 and 22.6 mol% Fs. Although, all components in the studied thin sections are recrystallized and have equilibrated silicates, the CT-image (Fig. 3d) shows chondritic components (perhaps chondrules) with elements of low mean mass. This may indicate the existence of Fe-poor, unequilibrated areas within the bulk rock of fragment R1.

Plagioclase occurs as quite large crystals sometimes exceeding 100 µm in size. Mean plagioclase has An- and Or-components of 9.8 ± 0.6 and 3.9 ± 2.6 mol%, respectively (n = 10; Table 2). The compositions vary between 8.6 and 10.7 mol% An. Both phosphates, merrillite and apatite, were found in the thin sections. A millimeter-sized, honey-yellow area on the broken surface of the chondrite breccia turned out to be phosphate-rich area having merrillite as the most abundant phase (Figs. 4a,b and S3). The major element compositions of the phosphates are listed in Table 2. The apatite is richer in F compared to apatites in other ordinary chondrites and similar to apatites in eucrites (e.g., Ward et al., 2017; Barnes et al., 2019). From this assemblage within thick section PL18087 the trace element concentrations of both phosphates were obtained by LA-ICP-MS (Table 3). The REE concentrations are presented in Fig. 7. Small grains of metals and sulfide occur throughout the entire thin sections (Table 4). However, large metallic phases are heterogeneously distributed and up to 200 µm in apparent size. Fig. 5d shows an area with a relatively high abundance of

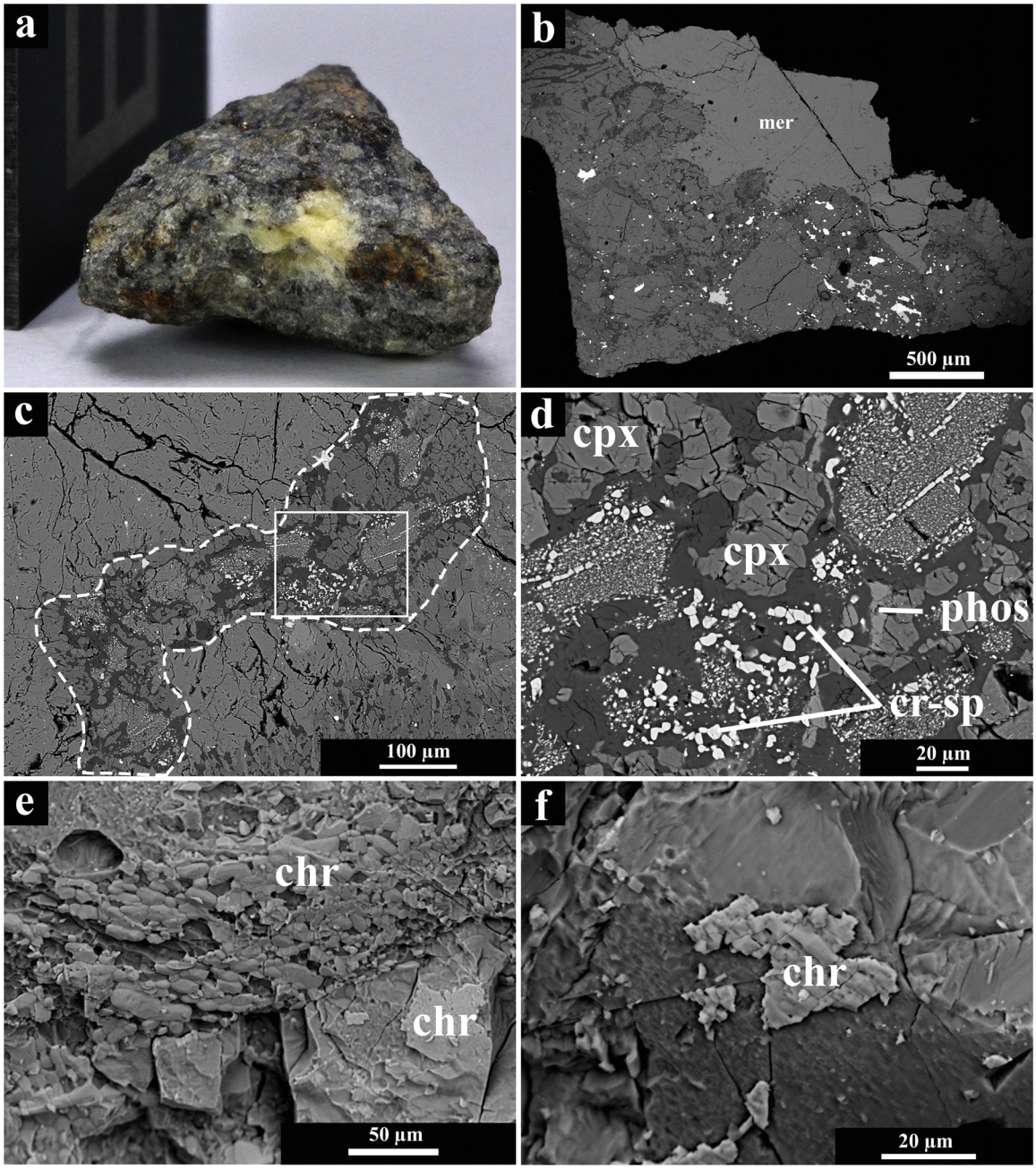


Fig. 4. (a) Within this 0.3 g fragment of Renchen a mm-sized honey-yellow area was detected. (b) In a polished thick section (PL18087) these areas turned out to consist of phosphates. Merrillite is by far the most abundant phosphate. (c,d) Recrystallized fine-grained, spinel-rich CAI with abundant plagioclase (dark grey) enclosing Ca-pyroxene (cpx), Ca-phosphate (phos), and areas rich in Cr-spinel (cr-sp; white). (e,f) At the broken surface different morphologies of chromite (chr) are visible. (b–f): Backscattered electron imaging.

such large metals and, by CT-studies, a huge metal blob of 3.24 mm has been identified in fragment R2 (Fig. 5b). In general, the metal grains are blurry in the electron optical image, heterogeneous in compositions, and include kamacite, taenite, and tetrataenite (Fig. 8). The Ni and Co concentrations of kamacite vary considerably (5.4–7.7 and 1.2–2.4 wt %, respectively). Also, the taenite composition is variable, with Ni content varying from 18 to 33 wt% and Co concentrations between 0.5 and 2.2 wt% (Table 4). We cannot rule out that the variations in the metals are related to shock processing (S4), since the rock has abundant melt areas and melt veins penetrating the fragments (see below).

Using CT, four phases of the meteorite are distinguishable within the slices of R1 (Fig. S1): air (pores, cracks), bulk silicates, metals, and sulfide. The total volume of the analyzed sample is 3552 mm^3. The volume of metals is 113 ± 29 mm^3 or 3.2 ± 0.8 vol%. The volume of sulfides (troilite) is 235 ± 74 mm^3 or 6.6 ± 2.1 vol%. The troilite in Renchen is also distributed throughout all thin sections. Large grains are shown in Figs. 5 and S1. Chromite occurs as grains of variable size and has mean MgO, Al_2O_3, and TiO_2 concentrations of 2.4 wt%, 5.5 wt %, and 3.0 wt%, respectively (n = 4; Table 2). They are frequently observed within all fragments. However, high abundance of chromite was found within a recrystallized Ca,Al-rich inclusion (CAI; Fig. 4). This object consists of abundant Ab-rich plagioclase, Ca-pyroxene, Ca-phosphate, and compact Cr-spinel-rich, fine-grained areas (Fig. 4). A typical area shown in Fig. 4d was analyzed by SEM/EDS and the composition revealed high abundances of Al_2O_3 (~13 wt%), Cr_2O_3 (~7 wt%), CaO (~7 wt%), and Na_2O (~6 wt%; compare Table 2). Areas rich in chromite were also found by investigating the surface morphology of the uncoated sample (Figs. 4e and 4f).

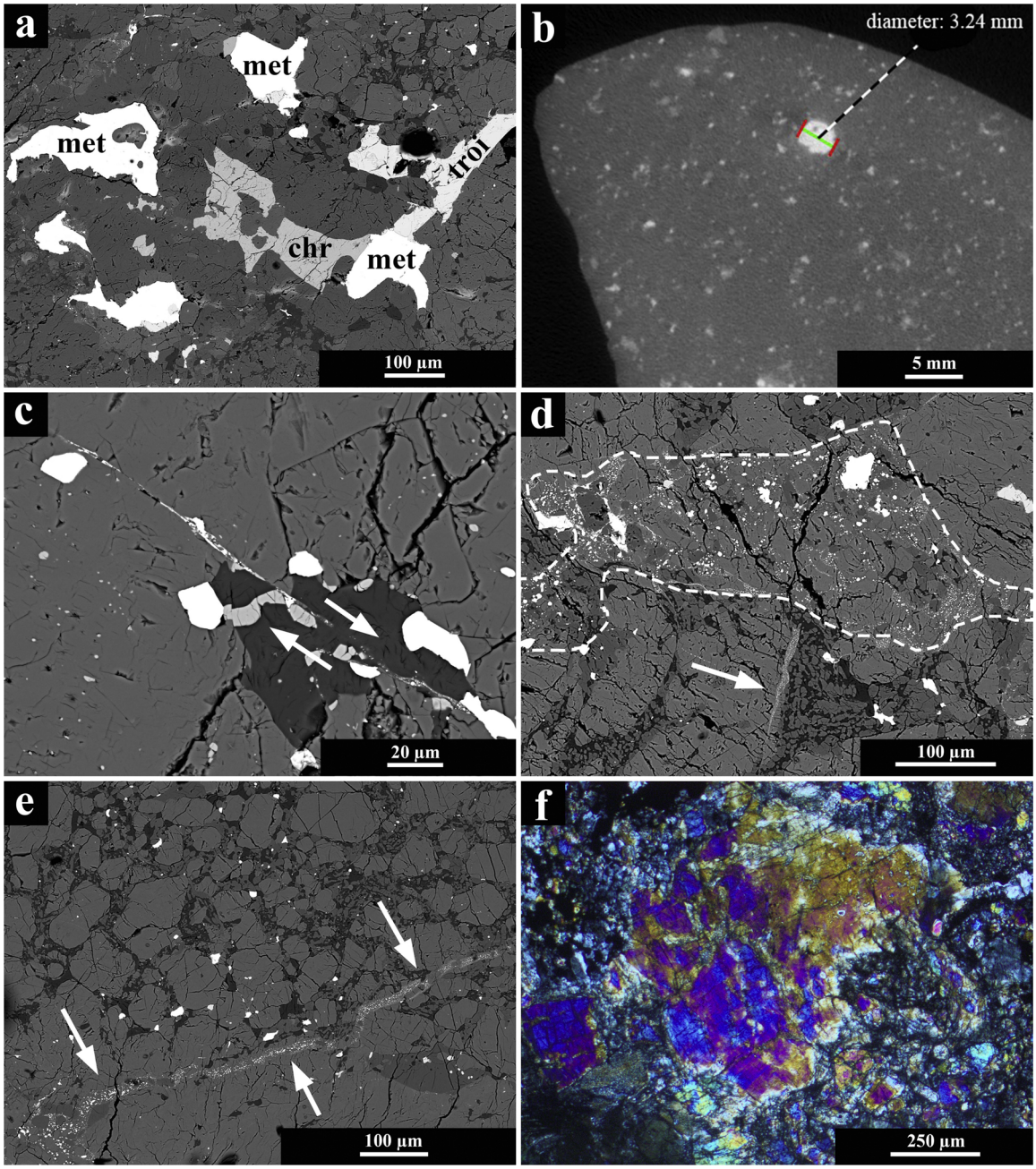


Fig. 5. (a) Area rich in opaque minerals including metals (met), troilite (tro), and chromite (chr). (b) CT slice-image of parts R2 showing the largest metal blob. (c) Small shock plane (visible as a vein) in Renchen indicating shift of matter along the shearing plane. (d) Locally, melted areas are observed between fragments. Sometimes fine-grained melt veins penetrate the fragments (arrow). (e) Impact melt clast with a shock vein (arrows). (f) Olivine shows weak mosaicism indicating a shock stage of S4. Images (a) and (c–e) in back-scattered electrons; (b): CT-image; (f): polarized light, crossed Nicols.

By X-ray element mapping of the broken, rough surface carbon-rich zones close to olivine (Fig. S4) were detected, however, the phase and origin of the C-bearing object remains unclear.

3.2.3. *Shock metamorphism and weathering*

As stated above, based on the study of the polished sections, Renchen is brecciated (Figs. 3 and 5). The breccia is well-lithified having abundant melt areas around and within its fragments (Fig. 5d). Sometimes, these fine-grained melt veins penetrate the fragments. In other cases dislocation of material along a shearing plane in visible (Fig. 5). Olivine and plagioclase show characteristic shock features. Generally, the olivine grains show weak mosaicism, while plagioclase shows undulatory extinction. High pressure phases (such as ringwoodite) were searched for by Raman spectroscopy, but could not be detected even in the melt veins. Some feldspar-glass or maskelynite is restricted to the shock veins and the occurrence was clearly proven by Raman spectroscopy (Fig. 9). In some of these areas crystalline relicts still exist (mixed zones). The optical and Raman features indicate that the rock is moderately-shocked (S4; Stöffler et al., 1991; Bischoff and Stöffler, 1992; Langenhorst et al., 2017). This shock stage (S4) is the most abundant shock degree among the L chondrites (Bischoff et al., 2019). Shock veins observed within the bulk sample cross-cut the various lithologies of Renchen (Fig. 5).

The residence time of 14 days on the ground resulted in first signs of terrestrial weathering. Areas with a brownish taint are locally already present resulting from the first breakdown of metals. Thus, a few rusty spots are clearly recognizable with the naked eye on the surface of the samples (compare Figs. 2 and 4a).

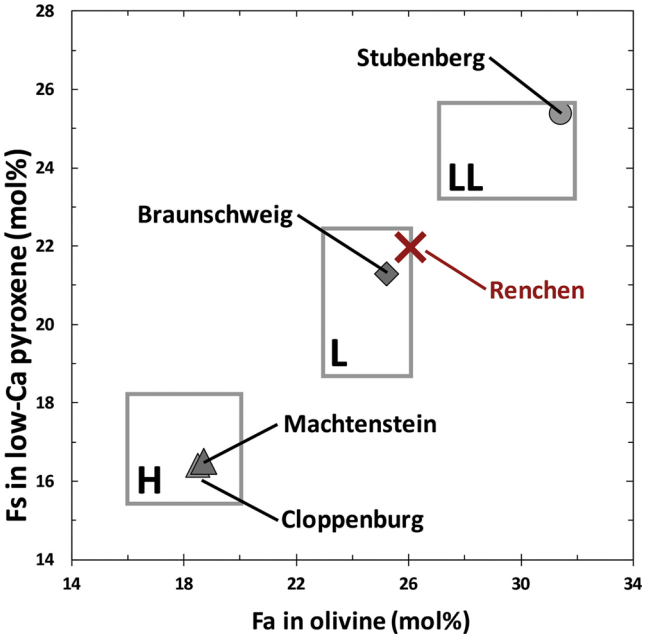


Fig. 6. Fa- and Fs-contents of olivine and low-Ca pyroxene of the Renchen L5-6 chondrite breccia. The fields for H-, L, and LL-chondrites are defined based on data from Gomes and Keil (1980) and Weisberg et al. (2006) for pyroxene and olivine, respectively. Also included are data concerning the recent German falls Braunschweig (Bartoschewitz et al., 2017) and Stubenberg (Bischoff et al., 2017a) and finds Machtenstein (Hochleitner et al., 2015) and Cloppenburg (Storz et al., 2017).

3.3. Chemical characteristics

3.3.1. Bulk chemistry

A small fragment of about 0.3 g was provided for chemical characterization. The results, summarized in Table 3 and shown in Fig. 10, indicate that for most elements the chemical composition of Renchen is close to the compositions of Braunschweig and other L chondrites (Lodders and Fegley, 1998; Bischoff et al., 2011; Bartoschewitz et al., 2017). Thus, the Renchen chondrite is most likely an L chondrite. However, there are also differences concerning the concentrations of some elements (e.g., Ni, P, Cr) compared to those in average bulk L chondrites that will be discussed below.

3.3.2. Noble gases

The noble gas results for the two fragments of Renchen are given in Tables 5a–5d. Concentrations of He and Ne, and particularly the most diagnostic Ne isotope composition, show no evidence for solar wind (Fig. 11). The light noble gases He-Ar contain essentially cosmogenic (cos) noble gases (only ^{38}Ar was corrected for ~2% of trapped ^{38}Ar) with additions of radiogenic ^{4}He and ^{40}Ar. The measured ^{3}He and ^{21}Ne can directly be used to determine cosmic-ray exposure (CRE) ages. The error-weighed ^{22}Ne/^{21}Ne (cos) is 0.8770 ± 0.0031, which is used as "shielding indicator" to determine the production rates with the chemistry- and shielding-depending model predictions by Leya and Masarik (2009). We used the bulk chemistry in Table 3 to calculate the productions rates P_3, P_{21} and P_{38}, which are given in Table 5e. The ^{22}Ne/^{21}Ne ratio suggests very low shielding depths of 1–10 cm in objects between 10–150 cm (and some very deep positions in an unlikely 5 m radius object that we can safely rule out). If we use the pre-atmospheric size constraint obtained from the radionuclide ^{26}Al (see below), we could narrow the "allowed" radii down to 10–20 cm. However, this will not significantly change the production rates for the noble gases, which only will significantly change within depth. The CRE ages including our "best guess" of ~42 Ma are given in Table 5e.

3.3.3. Radionuclides

The activities for the very short-lived radionuclides and the naturally occurring radionuclides are given in Table 6 and are in agreement with the average concentrations in ordinary L chondrites (Wasson and Kallemeyn, 1988). From ^{26}Al (Leya and Masarik, 2009) and ^{22}Na (Bhandari et al., 1993) a size of the parent body of < 20 cm and 15–100 cm can be derived. The naturally occurring radionuclides are in agreement with the average concentrations in ordinary L chondrites (Wasson and Kallemeyn, 1988). The ^{22}Na/^{26}Al of (1.7 ± 0.2) is compatible with the one expected for L chondrites averaged over a solar cycle (Bhandari et al., 2002).

3.3.4. Oxygen isotopes

The oxygen isotope compositions of the two analyzed fragments of Renchen are $\delta^{17}O$ = 3.54 and 3.71‰ and $\delta^{18}O$ = 4.65 and 4.82‰, respectively, resulting in a mean of $\delta^{17}O$ = 3.63‰ and $\delta^{18}O$ = 4.74‰ (Fig. 12). This gives an offset in $\delta^{17}O$ of $\Delta'^{17}O$ = 1.12‰ relative to a reference line with a slope of 0.5305 (Wiechert et al., 2001; Pack and Herwartz, 2014; Herwartz et al., 2014; Pack et al., 2017). The data for Renchen are consistent with those of other L chondrites.

3.3.5. Titanium isotopes

The Ti isotope composition for Renchen samples measured in

Table 2
Chemical composition of main phases and the metamorphosed CAI (area shown in Fig. 4d) in the Renchen fragmental breccia. All data in wt%; n.d. = not detected; n.a. = not analyzed; n = number of analyses. *) contains about 3.4 wt% F.

wt%	Olivine	Pyroxene	Ca-Pyroxene	Plagioclase	Apatite	Merrillite	Chromite	CAI
	n = 59	**n = 21**	**n = 7**	**n = 10**	**n = 6**	**n = 17**	**n = 4**	
SiO_2	37.9	55.2	53.9	66.0	< 0.03	< 0.01	< 0.03	48.5
TiO_2	< 0.02	0.22	0.50	< 0.03	n.d.	n.d.	2.98	0.47
Al_2O_3	< 0.01	0.18	0.56	21.1	< 0.01	< 0.01	5.5	13.1
Cr_2O_3	< 0.02	0.16	0.87	< 0.01	< 0.02	< 0.01	55.7	7.2
FeO	23.8	14.5	4.8	0.50	0.07	0.43	31.3	7.5
MnO	0.48	0.48	0.20	< 0.01	< 0.02	< 0.02	0.71	0.26
MgO	37.7	28.5	16.6	< 0.04	< 0.03	3.5	2.43	8.8
CaO	< 0.02	0.71	21.7	1.99	54.9	46.6	n.d.	7.0
Na_2O	< 0.01	< 0.02	0.59	9.7	n.d.	2.71	< 0.02	6.3
K_2O	< 0.01	< 0.01	n.d.	0.66	n.d.	< 0.04	< 0.01	0.59
P_2O_5	< 0.04	< 0.01	n.a.	< 0.01	41.4	46.2	n.d.	1.09
Cl	< 0.01	< 0.01	n.a.	n.d.	0.47*	n.d.	n.a.	n.d.
Fa	26.1 ± 0.5							
Fs		21.9 ± 0.3	7.6 ± 0.7					
Wo		1.4 ± 0.3	44.8 ± 0.6					
An				9.8 ± 0.6				
Or				3.9 ± 2.6				

Table 3
Trace and major element abundances of Renchen (Ren) and of merrillite and apatite of the mm-sized assemblage shown in Figs. 4a,d. (*) data in wt%, other data in ppm. Data for Braunschweig are from Bartoschewitz et al. (2017). For the concentration of major elements of the phosphates see Table 2. Relatively high concentrations of Th and U in the bulk measurement of Renchen may result from the inhomogeneous distribution of large phosphate aggregates (see Figs. 4a,b).

Element	Renchen L5-6	Braunschweig L6	Cloppenburg H4-5	Apatite (Ren) Mean [n = 5] ± 1σ	Merrillite (Ren) Mean [n = 17] ± 1σ
Al	1.01*	1.159*	0.95*		
Fe	21.5*	21.6*	23.5*		
Mg	16.65*	15.0*	12.79*		
Na	0.54*	0.712*	0.19*		
Ni	0.91*	1.23*	1.38*		
P	844	1310	1450		
K	907	1021	667		
Ca	1.33*	1.41*	0.93*		
Si				855 ± 220	434 ± 66
Sc	9.13	10.01	8.03	1.5 ± 1.1	5.06 ± 0.26
Ti	634	644	577	< 19	13.6 ± 2.3
V	70.3	70.09	78.8	< 0.97	2.94 ± 0.28
Cr	4372	3804	4139	< 7.1	8.4 ± 2.0
Mn	0.30*	0.267*	0.25*	157 ± 38	176.0 ± 9.2
Co	518	601	635	< 0.49	0.261 ± 0.067
Zn	29.9	43.96	46.8		
Ga	4.11	5.05	4.55		
As				< 7.1	3.87 ± 0.76
Rb	2.73	3.06	1.65	< 0.42	0.731 ± 0.051
Sr	10.68	11.34	6.75	78.0 ± 3.4	43.0 ± 1.6
Y	2.14	2.32	2.14	75 ± 21	380.9 ± 3.5
Zr	5.69	6.48	5.96	48 ± 18	0.221 ± 0.040
Nb	0.494	0.46	0.479	0.081 ± 0.027	0.085 ± 0.012
Cs	0.088	0.048	0.022	< 0.16	< 0.043
Ba	4.17	3.78	4.00	0.85 ± 0.40	0.42 ± 0.15
La	0.317	0.328	0.368	27.8 ± 4.2	75.3 ± 1.0
Ce	0.816	0.873	0.915	61 ± 11	196.9 ± 2.5
Pr	0.162	0.128	0.134	8.3 ± 1.8	29.10 ± 0.30
Nd	0.757	0.649	0.653	36.2 ± 8.2	144.3 ± 2.1
Sm	0.195	0.218	0.205	10.3 ± 2.7	44.92 ± 0.78
Eu	0.0797	0.0827	0.0730	0.87 ± 0.13	2.330 ± 0.075
Gd	0.262	0.30	0.271	12.5 ± 3.5	59.65 ± 0.79
Tb	0.0498	0.0549	0.0505	2.01 ± 0.56	10.35 ± 0.11
Dy	0.337	0.378	0.339	12.7 ± 3.4	68.00 ± 0.83
Ho	0.0754	0.0835	0.0754	2.79 ± 0.77	14.65 ± 0.16
Er	0.225	0.250	0.223	7.6 ± 2.0	40.99 ± 0.59
Tm				1.00 ± 0.34	5.386 ± 0.076
Yb	0.230	0.256	0.219	6.6 ± 2.0	32.47 ± 0.55
Lu	0.0354	0.0392	0.0328	0.84 ± 0.23	4.288 ± 0.047
Hf	0.173	0.197	0.149	0.073 ± 0.040	0.0041 ± 0.0021
Ta	0.0253	0.0227	0.0228	< 0.011	0.00174 ± 0.00086
Pb	0.0658	0.0336	0.0485	4.3 ± 1.0	0.99 ± 0.13
Th	0.0650	0.0452	0.0485	11.4 ± 3.8	3.05 ± 0.14
U	0.0291	0.0128	0.0189	16.5 ± 5.6	0.274 ± 0.028

Münster and Zürich are ε^{46}Ti = -0.07 ± 0.08, ε^{48}Ti = 0.05 ± 0.08, ε^{50}Ti = −0.81 ± 0.15 (n = 7; Student-t 95% confidence interval) and ε^{46}Ti = −0.21 ± 0.06, ε^{48}Ti = −0.03 ± 0.03, ε^{50}Ti = −0.64 ± 0.08 (n = 12, $2\sigma_{SE,\ mean}$), respectively (Fig. 13).

3.3.6. Chromium isotopes

The Cr isotope data carried out at ETH Zürich yielded a Cr isotope composition for Renchen of ε^{53}Cr = 0.31 ± 0.04 and ε^{54}Cr = −0.25 ± 0.04. This composition falls on the extreme end of the field that is defined by ordinary chondrites (Fig. 13b; Bischoff et al., 2017a), but overlap within error with previous data of ordinary chondrites (Qin et al., 2010).

3.3.7. Solvent-soluble organic matter

The elements O, N, H, S, and C are the most abundant elements in the early Solar nebula and high abundances may have accreted as ices in the early-formed planetesimals. From very simple organic molecules such as formaldehyde (CH_3O), water (H_2O), methanol (CH_3OH), and ammonia (NH_3), a whole size and structural continuum of highly complex and diverse chemistry can evolve such as experimentally shown on cometary ice analogues (Theulé et al., 2013). The analysis of the methanol-soluble organic fraction of Renchen by ultrahigh resolution mass spectrometry resulted in exact masses that could be converted into 7900 elementary species in the CHNOS space and into 1400 CHOMg formulae with a CHOMg/CHO ratio of 0.5. These data are visualized in van Krevelen diagrams (see explanation above) in Fig. 14 by plotting the H/C ratio of each formula versus its O/C or m/z ratio, sizing the bubble size with the relative abundance of the signals.

3.4. Physical characteristics

3.4.1. IR-Spectroscopy

A mid-infrared bidirectional reflectance spectrum (incident and emergent angle of 20°) of a thin section (PL18089) of the Renchen meteorite compared to reflectance powder spectra of some other L5 and L6 meteorites taken from NASA RELAB spectral database is shown in Fig. 15. This infrared spectrum of the thin section of the Renchen meteorite demonstrates the occurrence of six clear bands between 8 µm and 14 µm indicated with gray lines in Fig. 15, which are comparable to the bands observable in the powder spectra of the other L5 and L6 meteorites. Spectra of the Renchen thin section taken at different viewing geometries with higher phase-angle show a higher overall

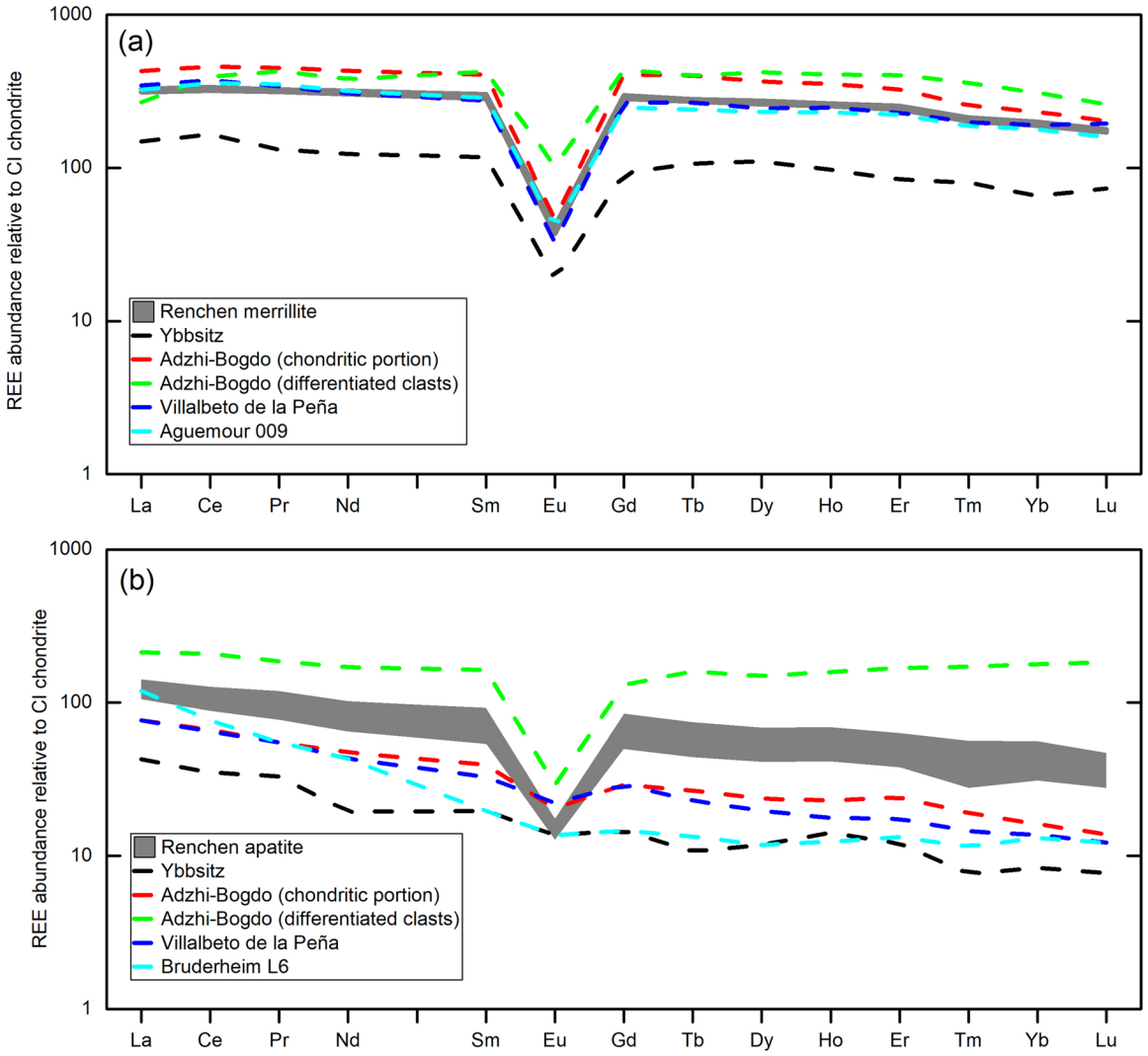


Fig. 7. REE-concentrations of (a) merrillite and (b) apatite from the assemblage shown in Fig. 4a,b normalized to CI (Barrat et al., 2012). The data for the other ordinary chondrites (H4, LL3-6, L6) are taken from Ward et al. (2017).

reflectance of the spectra with higher phase angle (Fig. S5). This is most probably the result of a stronger specular component in the spectra caused by the mirror-like surface of the thin section.

3.4.2. *Magnetic susceptibility and density*

The average values for the magnetic susceptibility (MS) of the samples, corrected for mass and dimensions, are given in Table 7 and shown in Fig. 16. The overall average value of log MS = 4.57 falls in between the ranges of L and LL chondrites.

The bulk density of the large piece R2 of 955 g was obtained. The measured volume of 281.2 ± 0.9 cm^3 revealed a density of 3.396 ± 0.011 g/cm^3. A density of almost 3.4 g/cm^3 rather suggests an L chondrite with a magnetic susceptibility perhaps lowered by shock phenomena. The analysis of the 228.2 g sample Renchen R6 sample revealed a density of 3.36 ± 0.025 g/cm^3. The somewhat lower density of R6, which was found about 6 months after the fall, may be related to some oxidation of metal due to terrestrial weathering. The average bulk densities for H, L, and LL chondrites are 3.42, 3.36, and 3.22 g/cm3, respectively (Consolmagno et al., 2008).

4. Discussion

4.1. *Mineralogical properties and classification of Renchen*

Renchen is a breccia based on presented results. The textures of most individual fragments are highly recrystallized (types 5 and 6;

Table 4
Chemical composition of metals and sulfide (troilite) in the Renchen fragmental breccia. All data in wt%. Data obtained by SEM-EDS and normalized to 100%.

	Kamacite (n = 7)		Taenite (n = 12)		Tetrataenite (n = 3)		Troilite (n = 6)	
	wt%	s.d.	wt%	s.d.	wt%	s.d.	wt%	s.d.
Fe	91.1	± 0.77	74.2	± 5.96	48.0	± 1.61	62.6	± 0.23
Ni	7.1	± 0.40	24.6	± 6.13	51.4	± 1.45	0.08	± 0.06
Co	1.74	± 0.35	1.18	± 0.40	0.43	± 0.10	0.24	± 0.08
S	n.d		n.d		n.d		37.0	± 0.15

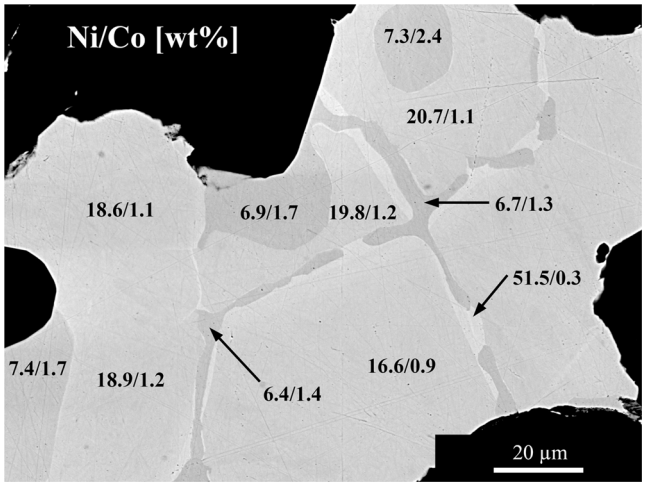


Fig. 8. Details of a metal aggregate within the Renchen breccia. The aggregate includes kamacite (~7 wt% Ni), taenite (~20 wt% Ni), and tetrataenite (~50 wt% Ni). The values "x.x/y.y" represent the Ni and Co-concentrations in wt% as obtained by SEM-EDS.

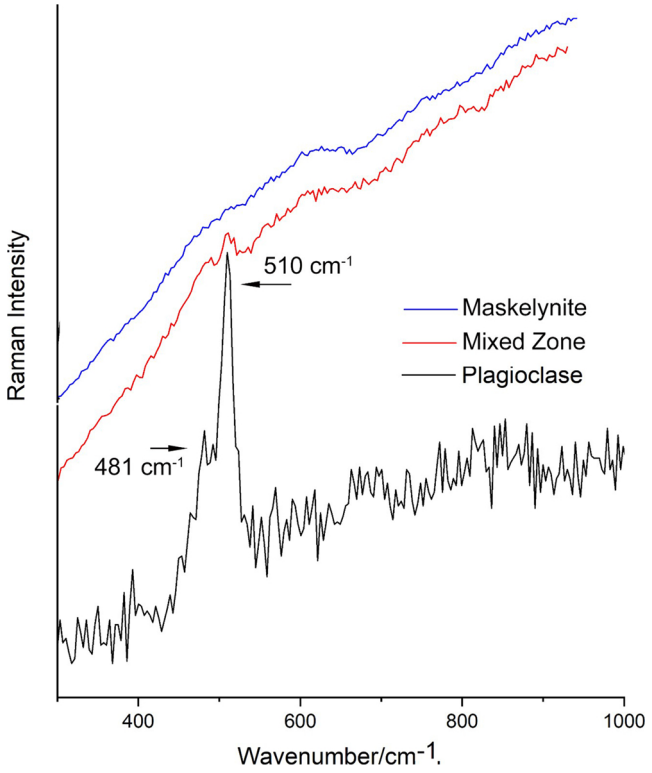


Fig. 9. Raman spectra of the plagioclase, a mixed zone, and maskelynite (diaplectic glass) in the wavenumber range from 300 cm^{-1} to 1000 cm^{-1}. Plagioclase **(black)** is identified by the two main peaks at 481 cm^{-1} and 510 cm^{-1}. In the mixed zone (red) a broadening of the peaks and increasing fluorescence is visible. The spectra are not background-corrected. The intensity increases due to an increase of fluorescence.

Fig. 3) and only recrystallized "relict" chondrules are visible in thin section (Fig. 3). These observations clearly point to a high metamorphic grade of the fragments within the rock. The grain size of plagioclase and the homogeneous compositions of olivines and pyroxenes also support this. Based on the mean olivine and low-Ca pyroxene compositions of $Fa_{26.1}$ and $Fs_{21.9}$, respectively, the rock is classified as an L-group ordinary chondrite breccia. However, it has to be noted that the mean compositions of olivine and low-Ca pyroxenes are at the high Fe-rich

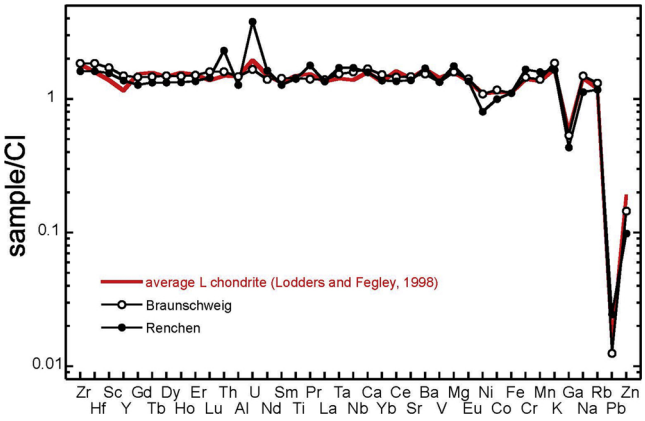


Fig. 10. Bulk composition of Renchen in comparison to the L chondrite Braunschweig (Bartoschewitz et al., 2017) and the average of other L chondrites (Lodders and Fegley, 1998). For normalization the CI-values of Barrat et al. (2012) are used.

end of mineral compositions in L chondrites (see Fig. 6). Since no fragments of other petrologic type have been observed in the thin sections so far a classification as a L5-6 breccia is appropriate. Besides the fragments of type 5 and type 6, the occurrence of impact melt clasts are clearly visible (Fig. 5f). The large metal rich-blobs visible in the images of the computed tomography (Fig. 5) may represent the metal-sulfide partial melts. However, Renchen does not belong to the complicated breccias like Kaidun or the 2008 TC_3 meteoroid (parent body of the Almahata Sitta rocks), which include many (> > 20) different meteorite classes and types (e.g., Zolensky et al., 1996, 2010; Zolensky and Ivanov, 2003; Bischoff et al., 2010; Horstmann et al., 2010; Goodrich et al., 2014; Horstmann and Bischoff, 2014) or to the complex regolith breccias among the L- and LL-group ordinary chondrites, which also contain different rock types (e.g., Bischoff et al., 1993, 2013a,2006,2018; Metzler et al., 2010, 2011). Renchen is also different to the LL5-6 breccia Chelyabinsk that contains genomict clasts of different petrologic types, as well as shock-darkened and impact melt lithologies (Bischoff et al., 2013b; Righter et al., 2015; Morlok et al., 2017). Considering the onion-shell model for the setting of the parent body, no clasts of lower petrologic type (3–4) originated from the near surface areas of the parent body were mixed into the breccia during impact-induced lithification (Kieffer, 1975; Bischoff et al., 1983).

During the CT-studies a metal abundance of 3.2 ± 0.8 vol% has been obtained, which is very similar to the mean metal abundance of 4 vol% for L chondrites (Weisberg et al., 2006). Considering the metal density (~8 g/cm^3) the Fe,Ni-metal value is well-above 6 wt%, which is within the range of L-group ordinary chondrites (Gomes and Keil, 1980). As mentioned above, the mean compositions of olivine and low-Ca pyroxenes are at the high Fe-rich end for L chondrites. Similarly, the relatively high Co-concentration in kamacite would probably be in the L/LL-range of Rubin (1990).

Based on the weak mosaicism in olivine within the entire rock the chondrite is moderately shocked (S4). Thus, Renchen is an L5–6, S4 ordinary chondrite breccia.

4.2. Formation of the Renchen breccia

The Renchen breccia represents a mixture of several lithic rocks including rock clasts of petrologic type 5 and type 6 and clasts of impact melt that were mechanically mixed and lithified by impact. Impact melts are the product of high stress (above 75–90 GPa) and temperature (above 1500–1750 °C) induced by impact processes (Stöffler et al., 1991). Typically, such melts quickly cool down on their parent asteroid (e.g., Rubin and Moore, 2011) and form a new melt lithology. This melt lithology can be fragmented again by impact and clasts could be mixed

Table 5a
Helium and Ne concentrations (in 10^{-8} cm^3 STP/g) and isotopic ratios in two samples of L5-6 Renchen.

	$^3He_{(cos)}$	^4He	$^3He/^4He$ × 10000	^{20}Ne	$^{20}Ne/^{22}Ne$	$^{21}Ne/^{22}Ne$	$^{21}Ne_{cos}$	$^4He_{rad}$
sample 1	65.3 ± 0.6	1619 ± 14	404 ± 5	11.37 ± 0.13	0.8190 ± 0.0039	0.8743 ± 0.0045	12.14 ± 0.14	1249 ± 33
sample 2	64.8 ± 0.6	1572 ± 14	412 ± 5	11.15 ± 0.13	0.8195 ± 0.0044	0.8796 ± 0.0043	11.97 ± 0.14	1205 ± 33

Table 5b
Argon concentrations (in 10^{-8} cm^3 STP/g) and isotopic ratios in two samples of L5-6 Renchen.

	^{36}Ar	$^{36}Ar/^{38}Ar$	$^{40}Ar/^{36}Ar$	$^{36}Ar_{tr}$	$^{38}Ar_{cos}$	$^{40}Ar_{rad}$
sample 1	1.272 ± 0.016	0.7319 ± 0.0062	2389 ± 61	0.162 ± 0.042	1.707 ± 0.0074	2991 ± 88
sample 2	1.065 ± 0.015	0.7247 ± 0.0078	2831 ± 75	0.125 ± 0.036	1.446 ± 0.0063	2979 ± 91

Table 5c
Krypton concentrations (in 10^{-10} cm^3 STP/g) and isotopic ratios in two samples of L5-6 Renchen.

	^{84}Kr	$^{78}Kr/^{84}Kr$	$^{80}Kr/^{84}Kr$	$^{82}Kr/^{84}Kr$	$^{83}Kr/^{84}Kr$	$^{86}Kr/^{84}Kr$
		^{84}Kr = 100				
sample 1	0.6614 ± 0.0084	1.91 ± 0.16	7.42 ± 0.25	23.73 ± 1.23	27.90 ± 1.26	26.99 ± 1.27
sample 2	0.5333 ± 0.0094	2.00 ± 0.19	8.05 ± 0.42	26.19 ± 1.50	28.99 ± 1.92	31.54 ± 1.35

Table 5d
Xenon concentrations (10^{-10} cm^3 STP/g) and isotopic ratios in two samples of L5-6 Renchen.

	^{132}Xe	$^{124}Xe/^{132}Xe$	$^{126}Xe/^{132}Xe$	$^{128}Xe/^{132}Xe$	$^{129}Xe/^{132}Xe$	$^{130}Xe/^{132}Xe$	$^{131}Xe/^{132}Xe$	$^{134}Xe/^{132}Xe$	$^{136}Xe/^{132}Xe$
		^{132}Xe = 100							
1	1.272 ± 0.016	0.521 ± 0.044	0.665 ± 0.041	8.09 ± 0.13	117.11 ± 1.66	16.37 ± 0.45	83.14 ± 2.03	38.82 ± 1.02	32.34 ± 0.64
2	1.065 ± 0.015	0.710 ± 0.074	0.838 ± 0.061	8.62 ± 0.24	157.65 ± 2.45	16.44 ± 0.51	83.54 ± 2.41	40.17 ± 1.21	33.51 ± 0.70

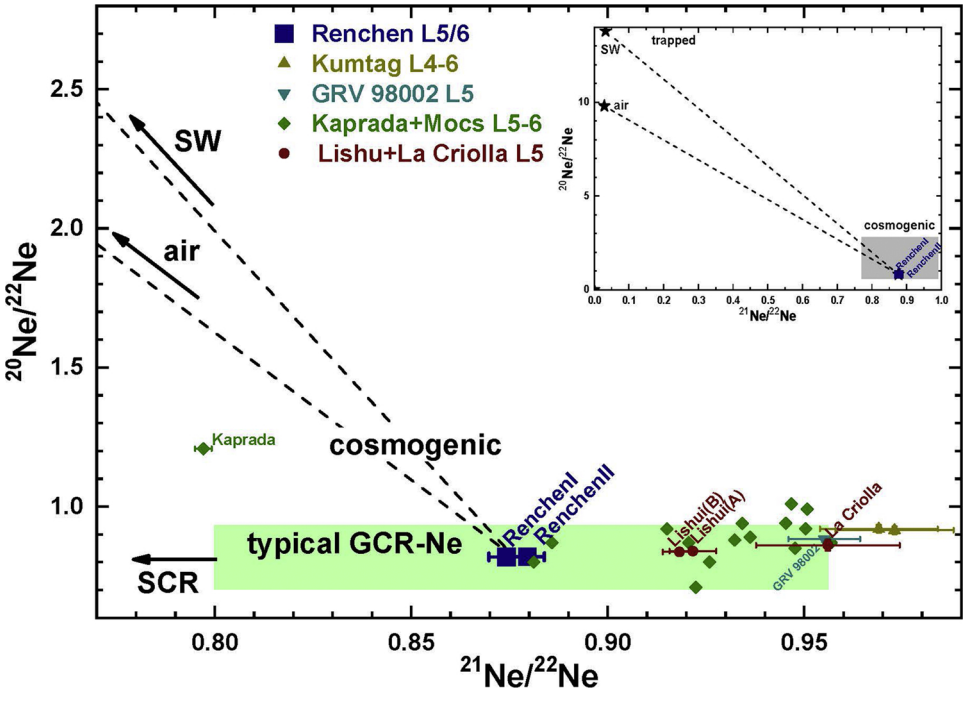


Fig. 11. Neon three isotope plot showing that the Ne in Renchen is completely cosmogenic. No trapped Ne (e.g. air or solar wind) is present. For comparison bulk data for other, similar L chondrites are shown. References: SW: Heber et al., 2009, GCR-Ne: Wieler, 2002, Kumtag: Zeng et al., 2018, GRV 98002: Lorenzetti et al., 2003, Kaprada: Bhandari et al., 2009, Mocs: Ferko et al., 2000, Lishu and La Criolla: Eugster et al., 1993.

together with other parent body lithologies. This has been observed for Renchen. During a survey of 2280 ordinary chondrites fragments of impact melt were found within 55 brecciated chondrites (Bischoff et al., 2018). Considering the 947 L chondrites, 220 (23%) are brecciated meteorites and 28 of these contain impact melted lithologies: nine samples are impact melt breccias and 19 samples contain melt clasts (Bischoff et al., 2018). Consequently, the Renchen meteorite belongs to the ~10% of impact melt-bearing breccias among the L chondrites. The Renchen impact melt clasts are characterized by well-equilibrated impact melt clasts. Thus, after formation of the impact melt, the crystallized impact melt were annealed and phases equilibrated prior to a subsequent impact that led to brecciation and mixing with the type 5

Table 5e
Cosmic ray exposure ages T_x determined for the two samples of L5-6 Renchen and production rates P_x determined based on the shielding indicator $^{22}Ne/^{21}Ne = 0.8770 \pm 0.0031$ (implying 10–150 cm radius, 1–10 cm depth) and the chemistry given in Table 3 with the model by Leya and Masarik (2009). P_x and respective ages in italics are given for comparison for the average L chondrite chemistry by Lodders and Fegley (1998).

	P_3 $cm^3/(g \times Ma)$	P_{21}	P_{38}	T_3 Ma	T_{21}	T_{38}	preferred age
1	1.60 ± 0.10	0.280 ± 0.018	0.0372 ± 0.0021	40.9 ± 2.7	43.4 ± 2.9	45.9 ± 2.7	**42 ± 3**
	1.50 ± 0.19	*0.272 ± 0.040*	*0.0357 ± 0.0053*	*43.4 ± 5.6*	*44.6 ± 6.6*	*47.8 ± 7.1*	
2	(see 1)			40.5 ± 2.6	42.8 ± 2.9	38.9 ± 2.3	
				43.1 ± 5.5	*44.0 ± 6.5*	*40.5 ± 6.0*	

Table 6
Massic activities (corrected to the fall of the meteorite July 10, 2018) of cosmogenic radionuclides (in dpm kg-1) and concentration of primordial radionuclides (ppb for U and Th chains and ppm for K_{nat}) in the specimens R2 and R6 of the Renchen stone measured by non-destructive gamma-ray spectroscopy. The much higher ^7Be concentration of R6 can potentially be attributed to environmental conditions on Earth; most likely, it is a surface contamination. Errors include a 1σ uncertainty of 10% in the detector efficiency calibration from Monte Carlo simulations (n.d. = not determined).

Nuclide	Half-life	R2 (955 g)	R6 (228.2 g)
^{48}V	15.9735 d	24.6 ± 3.1	Not visible
^{51}Cr	27.704 d	59.0 ± 10.6	Not visible
^{7}Be	53.22 d	149.5 ± 6.5	665 ± 116
^{58}Co	70.83 d	6.4 ± 0.8	Not visible
^{56}Co	77.236 d	6.8 ± 0.8	Not visible
^{46}Sc	83.787 d	11.1 ± 1.2	Not visible
^{57}Co	271.8 d	9.5 ± 1.3	7.1 ± 1.4
^{54}Mn	312.3 d	84.5 ± 8.9	55.9 ± 5.7
^{22}Na	2.60 y	106.7 ± 1.3	82.6 ± 8.4
^{60}Co	5.27 y	< 0.4	0.6 ± 0.3
^{44}Ti	60 y	n.d.	n.d.
^{26}Al	7.17×10^5 y	64.7 ± 6.8	56.1 ± 5.7
Primordial nuclide			
U		16 ± 1	13 ± 1
Th		44 ± 3	45 ± 4
K		1037 ± 62	865 ± 52

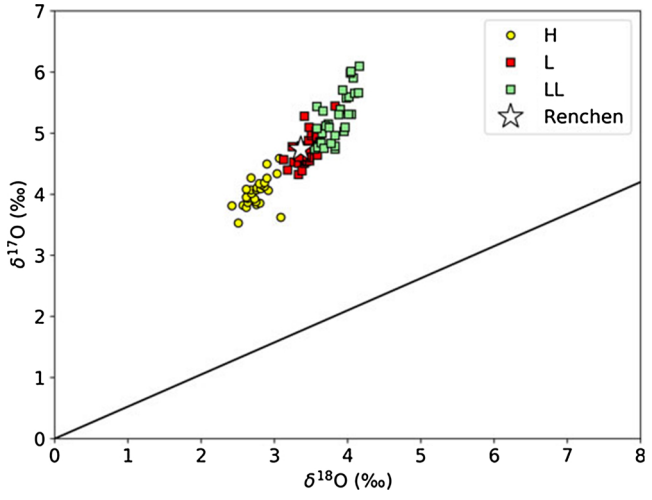


Fig. 12. The O-isotope data for Renchen are consistent with those of other L chondrites. The solid line is the Terrestrial Fractionation Line (TFL).

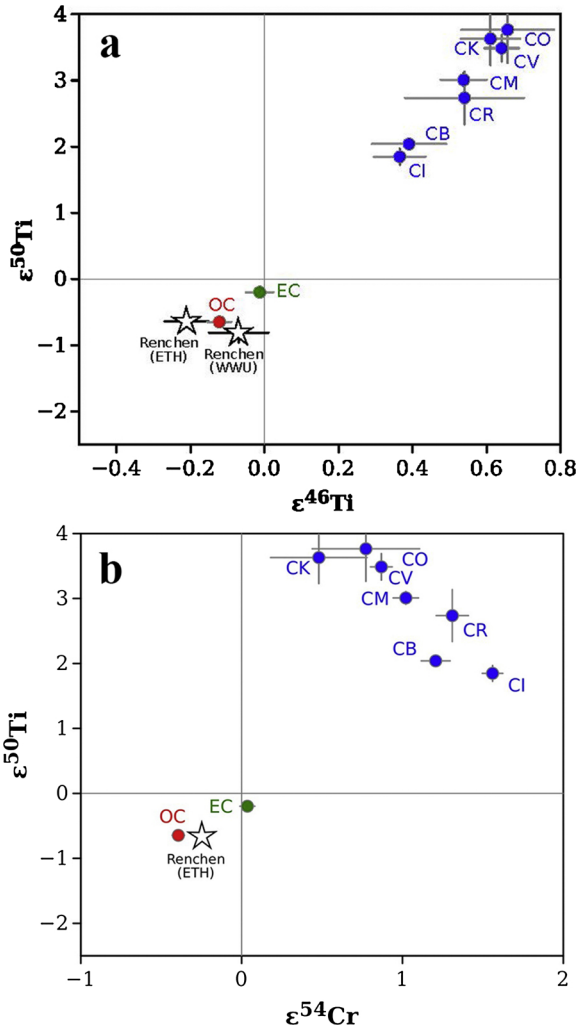


Fig. 13. (a) Ti isotope composition for Renchen samples measured in Münster (WWU) and Zürich (ETH). These values are consistent within uncertainty with each other and average literature data for ordinary chondrites ($\varepsilon^{46}Ti$ = -0.12 ± 0.03, $\varepsilon^{48}Ti$ = 0.00 ± 0.06, $\varepsilon^{50}Ti$ = -0.65 ± 0.07; Burkhardt et al., 2017; also see for original data from Trinquier et al. (2009); Zhang et al. (2012), and Williams (2015)); (b) Ti versus Cr isotope data for various meteorite groups and Renchen (star). Each group occupies a unique space in the diagram. Renchen falls in the area of ordinary chondrites. Compilation of literature data from Burkhardt et al. (2017).

and type 6 parent rocks. The components were lithified by shock (Kieffer, 1975; Bischoff et al., 1983). After lithification, the parent asteroid experienced another shock event producing shock melted areas such as the shock veins shown in Fig. 5 that are not restricted to distinct lithologies, but cross-cut all existing lithologies (Fig. 5f). Thus, this reaccreted and re-lithified rock certainly represents an impact-induced, second-generation parent body lithology and clearly demonstrates that several distinct collisional events are necessary in order to form the Renchen breccia.

4.3. Chemical properties of Renchen and its large phosphates

The bulk composition of the Renchen meteorite is very close to the

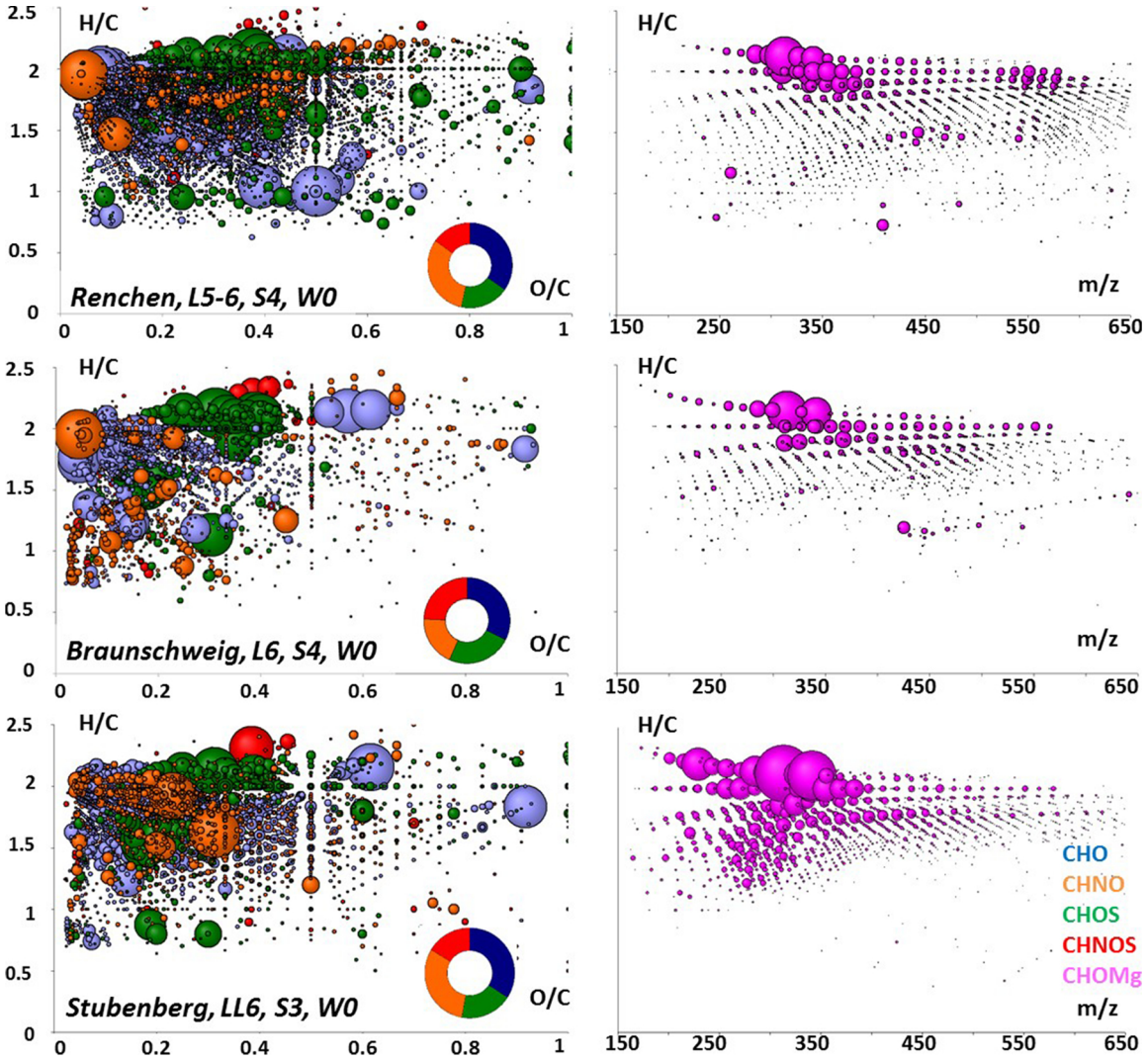


Fig. 14. Van Krevelen diagram visualization in the CHNOSMg space in the negative mode electrospray ionization FTICR-MS illustrates the exact mass data of the methanol soluble organic matter of Renchen, Braunschweig, and Stubenberg meteorites (Bartoschewitz et al., 2017; Bischoff et al., 2017a). The bubble size expresses the relative intensity of the thousands of signals in the experimental mass spectra; the colors in legends represent the components of the left-hand side of the figure (CHO, CHNO, CHOS, CHNOS) and of the right-hand side (CHOMg).

published concentrations of other metamorphosed L-group ordinary chondrites like Braunschweig and the average of other L chondrites (Table 3; Fig. 10; Lodders and Fegley, 1998; Bartoschewitz et al., 2017). It can be concluded that no anomalies in elemental composition of the Renchen meteorite were detected compared with other L-chondrites, although some deviations exist as mentioned above. The bulk Ni content of 0.915 wt% is lower than the average L-chondrite Ni-concentration of 1.24%. Also, the Ni/Co ratio of 17.6 is much below the Ni/Co ratio in L-chondrites of 21.4 listed by Lodders and Fegley (1998). These differences may be related to the inhomogenous distribution of metal within the sample as obtained by CT-studies (see above; Fig. 5b). The presence of large impact melt lithologies (Fig. 5e), the occurrence of unusually large phosphate assemblages (Figs. 4a,b) as well as the local enrichments in Cr-bearing minerals (Figs. 4c–f) in the breccia may also explain the somewhat unusual P- and Cr-concentrations in comparison with those of mean L chondrites (Lodders and Fegley, 1998).

Renchen is a very fresh sample and the chemical composition has not been affected by terrestrial alteration as it is the case for the Cloppenburg chondrite that has been analyzed for comparison (resulting in loss of e.g., Na, K, Rb, Sr).

The most abundant phosphates in ordinary chondrites are merrillite and Cl-apatite and are typically up to several hundred μm in size. A huge merrillite-apatite aggregate with almost two mm-sized merrillite enclosing some small apatites is the largest we ever saw in an ordinary chondrite. Different to apatites in other ordinary chondrites, which are Cl-rich (e.g., Ward et al., 2017), the grains within the aggregate are F-rich (Table 2). Considering the REE concentrations merrillites have higher concentrations than apatite. In the patterns of both phases a negative Eu-anomaly is observed and relative to CI the light REE are slightly enriched compared to the heavy REE. As stated by Ward et al. (2017) the presence of plagioclase in a given phosphate paragenesis influences the magnitude of negative Eu anomalies as Eu^{2+} is preferentially incorporated into plagioclase. The mean La-enrichment (LREE) compared to CI of La for merrillite and apatite is about 200x and ~100x, respectively, while the mean Lu-enrichment (HREE) in merrillite and apatite is ~115x and ~40x, respectively. The values for merrillite are exactly within the range of REE concentrations in merrillites from other ordinary chondrites like Villalbeto de la Pena or Bruderheim (Fig. 7; Ward et al., 2017). However, the REE-pattern of apatite slightly deviates from the apatite patterns in Villalbeto de la Pena or Bruderheim and is more similar to the REE patterns (with the pronounced negative Eu-anomaly; Fig. 7) found for apatite within the differentiated clasts from the Adzhi-Bogdo (stone), although apatites with similar REE patterns have been reported from other ordinary

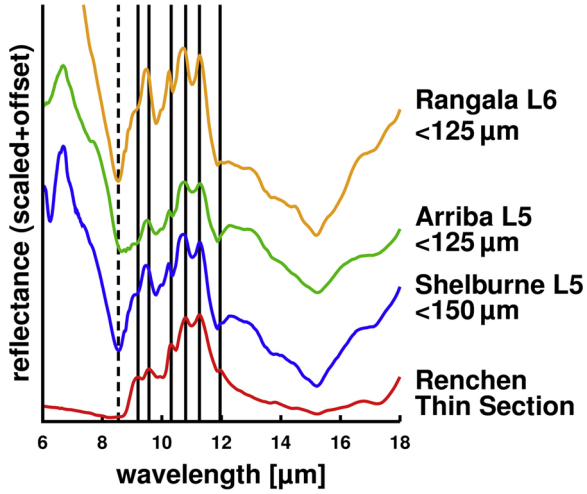


Fig. 15. IR-spectra of Renchen thin section PL18089 compared to other L5 and L6 meteorites taken from NASA RELAB spectral database. See text for explanation. The black dotted line indicates the Christiansen feature (CF) at around 8.54 µm (fitted to the CF of Rangala). Black lines indicate strong Reststrahlenbands (RB).

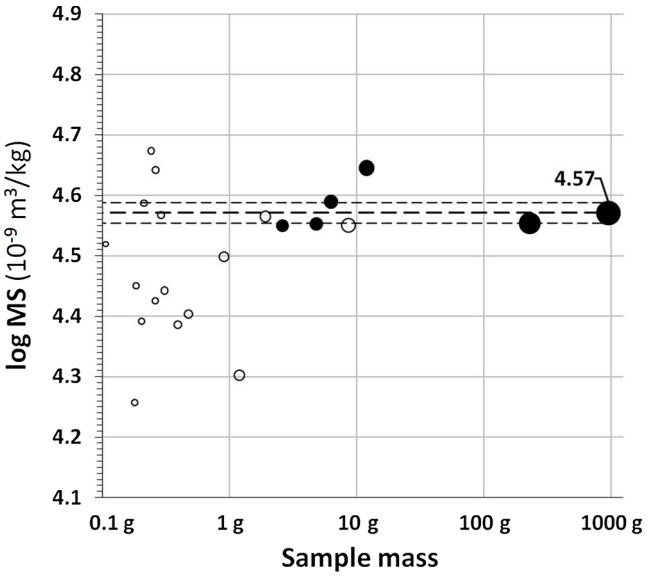


Fig. 16. Magnetic Susceptibility (MS) of Renchen meteorite fragments. The individuals are presented by full circles, while the fragments are indicated by open circles; dashed lines: main mass average with 95% confidence interval (compare Table 7).

chondrites (Crozaz et al., 1989). As also mentioned above, the high F concentration of the apatite deviates from F contents in grains of other ordinary chondrites and is similar to apatites in eucrites (e.g., Ward et al., 2017; Barnes et al., 2019). We have no explanation for this finding at the moment.

4.4. Renchen and the formation, abundance and nomenclature of organic components

This organic matter is grouped into soluble (SOM) and insoluble organic matter (IOM), whose chemical structures and variations are currently investigated using modern organic spectroscopy. During parent body processes, these insoluble and *soluble* organic matter further develop, depending on redox conditions driven by heat and/or aqueous alteration. They evolve along with the mineral phases allowing an incorporation of sulfur into the organic structures further increasing the complexity (Schmitt-Kopplin et al., 2010). Carbonaceous chondrites show the most pristine organic chemistry with the highest diversity in C,H,N,O,S-bearing molecules. Murchison (CM2) presents a diversity of millions of different compounds in the lower mass range up to 1000 amu. Further thermal and aqueous alteration may change the abundances and chemical species of the remaining soluble organics. Ordinary chondrites still contain ten thousands of different organic molecule structures and with increasing petrologic type they show the formation of covalently bond metals, especially Mg and are therefore termed “CHOMg” (Ruf et al., 2017).

Soluble organic species are intensively studied and recent investigations show that IOM and SOM are reacting instantaneously on small thermal annealing and pressure stresses. Several aspects were observed:

Table 7
Magnetic Susceptibility (MS) of the Renchen meteorite fragments.

#	Code	Sample	Number	Mass [g]	MS [10^{-9} m^3/kg]	log MS
1	20180710 BTR1	individual	R1	11.94	44182	4.645
2	20180710 BTR2	main mass	R2	955	37248	4.571
3	20180710 BTR3	individual	R4	4.82	35705	4.553
4	20180710 TKR1A	individual	R3S	2.60	35490	4.550
5	20180710 LSR1A	fragment	R3A	8.62	35525	4.551
6	20180710 LSR1B	fragment	R3B	1.91	36754	4.565
7	20180710 LSR1D	fragment	R3D	1.19	20063	4.302
8	20180710 LSR1E	fragment	R3E	0.90	31515	4.499
9	20180710 LSR1F	fragment	R3F	0.47	25316	4.403
10	20180710 LSR1G	fragment	R3G	0.39	24336	4.386
11	20180710 LSR1H	fragment	R3H	0.31	27700	4.442
12	20180710 LSR1I	fragment	R3I	0.29	36938	4.567
13	20180710 LSR1R	fragments set 1	R3R1	0.11	33055	4.519
14	20180710 LSR1R	fragments set 2	R3R2	0.03	43877	4.642
15	20180710 LSR1J	fragment	R3J	0.26	26634	4.425
16	20180710 LSR1K	fragment	R3K	0.21	38665	4.587
17	20180710 LSR1L	fragment	R3L	0.26	43800	4.641
18	20180710 LSR1M	fragment	R3M	0.18	28206	4.450
19	20180710 LSR1N	fragment	R3N	0.20	24618	4.391
20	20180710 LSR1O	fragment	R3O	0.24	47168	4.674
21	20180710 LSR1P	fragment	R3P	0.18	18088	4.257
22	20180710 MKR1	individual	R5	6.29	38873	4.590
23	20180710 TKR2	individual	R6	228.2	35762	4.553

a) With thermal annealing (metamorphism) the CHNOS- and CHOMg-components behave differently. The number of different organic CHNOS-species is decreasing along with the loss of volatile elements C, H, N, O, S. However, the number of N-bearing molecules, and the abundance and diversity of CHOMg-components increases with thermal metamorphism (Popova et al., 2013; Jenniskens et al., 2014; Kerraouch et al., 2019). As an example, a type 6 ordinary chondrite (like Braunschweig or Stubenberg; Bartoschewitz et al., 2017; Bischoff et al., 2017a) has a much higher abundance of distinct CHOMg-components as a type 3 ordinary chondrite, although the concentration and abundance of CHNOS-species is lower. These trends are simply visualized in Fig. S6.
b) A low-temperature processed CI or CM chondrite has far less-developed (low number) of distinct in CHOMg organic species, but a high abundance of CHONS-components.
c) Shock metamorphism also increases the number of different CHOMg species. This is especially the case considering shock processing in excess of 30–40 GPa producing significant impact-induced annealing (post shock heating).

As the main result on the Renchen analysis Fig. 14 clearly shows that the sample belongs to the metamorphosed samples having a high abundance of distinct CHOMg-components. Shock may also be responsible for this high abundance of these species as observed in ongoing studies. As a consequence, the study of the *soluble* organic components is more sensitive than the *insoluble* organic matter (IOM) to slight stresses and may be used in future to characterize the thermal history of a rock and may become an additional parameter for classification of the petrologic types of chondrites. More evidences still have to be accumulated to understand the intimate processes and constraints in the novel organic chemistry discovered in meteorites. However, more basic work and an improved database are urgently needed.

4.5. Noble gases significance

The light cosmogenic noble gases in both Renchen fragments yield, within uncertainties a cosmic ray exposure age of ~42 Ma. A complex history with additional exposure of Renchen on the L chondrite parent body is not discernible. A slight shift to lower ages with lighter mass might be visible, which could indicate some minor loss by heating either during the meteoroid's transport through space or atmospheric entry. However, we consider this unlikely, particularly in view of the potentially slightly too low P_{38}. The production rates determined by Leya and Masarik (2009) do not contain the production of ^{38}Ar from K. This could affect the production rates by perhaps 10–15 % (Cressy and Bogard, 1976; Freundel et al., 1986) and could account for some of the observed variations (cf. Di Gregorio et al., 2019) and could move the ^{38}Ar CRE ages accordingly slightly down.

Our preferred CRE age of 42 Ma places Renchen among the large number of members of the L chondrite group which were ejected around 40 Ma ago (Marti and Graf, 1992; Herzog and Caffee, 2014).

Consistent with Renchen's classification, it contains almost no trapped Ar, Kr and Xe (Tables 5a–5d). Only ~12.5% of the ^{36}Ar is trapped, based on the decomposition of the measured Ar between Ar_{cos} with $(^{36}Ar/^{38}Ar)_{cos}$ ~0.65 and Q/air with $^{36}Ar/^{38}Ar$ ~5.33. The small Kr and Xe amounts detected could be atmospheric, or remnants of Q gases that are more abundant in type 3 and 4 L chondrites and decrease quickly with metamorphic degree (e.g., Sears et al., 1980; Busemann et al., 2000). The precise Kr and Xe isotopic compositions are difficult to assess due to the large uncertainties, a result of the small gas amounts measured in the only ~30 mg samples. However, a small and not unusual excess compared to Q or air in ^{129}Xe due to the decay of short-lived ^{129}I is visible. Also, small deviations in the light isotopes, e.g., in the $^{124}Xe/^{132}Xe$ and $^{126}Xe/^{132}Xe$ ratios, are observed that are consistent with the presence of cosmogenic Kr and Xe.

Radiogenic ^{4}He and ^{40}Ar can be determined via $(^3He/^4He)_{cosm}$ ~0.2 and $^3He = {}^3He_{cos}$ and conservatively assuming that the trapped Ar is air, with $^{40}Ar/^{36}Ar$ ~296 rather than Q with $^{40}Ar/^{36}Ar$ ~0. The measured $^{40}Ar/^{36}Ar$ ratios are very high (2400–2800) and, hence, the correction for air is negligible. Using the K concentrations from Tables 3 and 6, we obtain a K-Ar retention age for Renchen of ~2.8-3.2 Ga. Renchen shows no evidence for a complete reset at the catastrophic event on the L chondrite parent body ~470 Ma ago that many L chondrites record (e.g., Haack et al., 1996; Korochantseva et al., 2007). The U/Th-^{4}He retention age is less well determined, because the U and Th concentrations determined here show considerable deviations (Tables 3 and 6). If we use both sets of U,Th concentrations, the U/Th-^{4}He retention age of Renchen is in the range 1.9 to 3.2 Ga. However, if we use only the U,Th concentrations obtained by gamma-ray spectroscopy, the U/Th-^{4}He age of Renchen in the range 3.0–3.2 Ga, which agrees with the age obtained from the K-Ar system. This is our preferred U/Th-^{4}He age, because the U,Th concentrations obtained by gamma-ray spectroscopy are essentially identical to the values given for average L chondrites (Lodders and Fegley, 1998).

4.6. Physical properties of Renchen

4.6.1. IR spectroscopy

The infrared spectrum of the thin section (PL18089) of the Renchen chondrite breccia (Fig. 15) shows the occurrence of six clear bands between 8 μm and 14 μm is well documented. Renchen mostly consists of olivine, low-Ca pyroxene, and albite-rich plagioclase. The visible bands in the Renchen spectrum result therefore from a mix of spectra of these components. The band located at 9.20 μm is dominated by the plagioclase component. The broad band at 9.57 μm is a superposition from features from all components, but the peak position is more indicative for the plagioclase. The feature at 10.32 μm is dominated by Ca-poor pyroxene and olivine. The bands at 10.80 μm and 11.26 μm are a strong superposition of the pyroxene and olivine components. The small band at 11.96 μm is strongly dominated by olivine.

The gray dotted line (Fig. 15) indicates the Christiansen feature (CF) at around 8.54 μm (fitted to the CF of Rangala), which is clearly visible in the powder spectra of the L chondrites Rangala, Arriba, and Shelburne, but not as clear in the Renchen thin section spectrum. Bischoff et al. (2017a) argued that the shifted and not very well-resolved CF in the Stubenberg meteorite is due to a less crystallized mesostasis feldspar in the meteorite compared to the other meteorites (see Salisbury (1993) for details). At the CF, a mineral or rock sample becomes more or less transparent for the infrared radiation. Metals are highly reflective in the mid-infrared wavelengths and polished metals act mirror-like. Therefore, the small polished metal fragments in the thin section are highly specular. In the Renchen spectrum a very small peak at 8.58 μm exists. Probably, this peak marks the "real" CF in Renchen and is therefore at a wavelength comparable to those of the other L5 and L6 meteorites in this study. Salisbury et al. (1991) found for the L group meteorites (two L3, two L5 and four L6) a mean wavelength of the CF of 8.65 μm. In their analysis the Shelburn meteorite was also included, but the CF of it was reported with a value of 8.64 μm, which is in contrast to the data taken from RELAB, for which we found a value of 8.54 μm for the CF. This discrepancy between the CF values of the RELAB spectra and our spectra to the spectra of Salisbury et al. (1991) is probably due to the measurement geometry. Salisbury and D'Aria (1989) showed that the usage of a biconical reflectance measurement geometry could shift the CF compared to directional hemispherical reflectance measurements. Usage of a collar in the beam path should avoid the CV from shifting by biconical reflectance measurements (Salisbury and D'Aria, 1989).

As mentioned above, spectra of the Renchen thin section taken at different viewing geometries with higher phase-angle show a higher overall reflectance with higher phase angle (compare Fig S5). This is most probably the result of a stronger specular component in the spectra caused by the mirror-like surface of the thin section. Also, the relative intensities of the reflectance features change. This effect could

be the result of the increased measurement point size, which is elliptical in size and varies from approximately 1.0 mm x 0.5 mm at an incident and emergent angle of 20° to approximately 2.6 mm x 0.9 mm at an incident and emergent angle of 70°. The field of view is therefore greater at higher phase angles and another composition of the analyzed sample is in the probed surface. The different behavior of the meteorite spectra in Fig. 15 below 8 µm are the result of the different sample types. Thin sections show a decreased reflectance at these wavelengths compared to powder spectra.

4.6.2. Density and magnetic susceptibility

The bulk density of almost 3.4 g/cm^3 rather suggests an L chondrite heritage with a magnetic susceptibility (MS) possibly lowered e.g. by shock processes. Compared to the log MS-values for the Stubenberg chondrite (LL6; 3.683 ± 0.015; Bischoff et al., 2017a) significantly higher values were determined for Renchen (4.57). One individual and the majority of small fragments deviate significantly from the average (see the Fig. 16), reflecting an inhomogeneous metal distribution. The size of the inhomogeneities partly exceeds 10 mm-scale. The inhomogeneous distribution of metal is well-documented by the CT investigations (compare Fig. 5b).

5. Conclusion

Renchen fell on July 10, 2018 and the first piece was recovered two weeks later, after an exact calculation of the impact area based on instrumental observations taken by several cameras of the Czech and German part of the European Fireball Network. Altogether six individuals weighing in total 1227 g were recovered until March 2019. The meteorite is classified as an L5-6, S4 ordinary chondrite fragmental breccia. The bulk composition of the Renchen meteorite is very close to element concentrations of other metamorphosed L-group ordinary chondrites. This is also consistent with O-, Ti-, and Cr-isotope data and IR spectroscopy. The measured activities of short-lived cosmogenic radionuclides clearly indicate that the analyzed pieces result from a very recent meteorite fall consistent with the Renchen fall. A cosmic ray exposure (CRE) age of 42 Ma has been obtained for the meteoroid. Using the K, U, and Th concentrations determined in this work U/Th-^{4}He ages K-^{40}Ar ages of ~3.0 to 3.2 Ga are determined.

Declaration of Competing Interest

The authors declare that they have no known competing financial interests or personal relationships that could have appeared to influence the work reported in this paper.

Acknowledgements

We thank U. Heitmann (Münster) for sample preparation and S. Ebert (Münster) for discussions and technical assistance. We also thank to Dr. Radmila Brožková from the Czech Hydrometeorological Institute (Prague) and Dr. Gerd Baumgarten of the Leibniz-Institute of Atmospheric Physics (Kühlungsborn) for providing wind models for this fall and the two anonymous reviewers for their helpful comments and suggestions, as well as the Associate Editor Falko Langenhorst. The work of P. Spurný was supported by Praemium Academiae from the Czech Academy of Sciences. M. M., P. M., and M. S. thank the Swiss National Science Foundation (SNF) for support. The work of H. B. is in parts supported by the NCCR "Planet S" funded by the Swiss SNF. A. B. and M. P. thank the DFG for support within the SFB-TRR 170 "Late Accretion onto Terrestrial Planets" (subproject B05; AB). This is TRR 170 publication No. 69. TZ and JK express thanks to the project CEITEC 2020 (LQ1601) for financial support from the Ministry of Education, Youth and Sports of the Czech Republic under the National Sustainability Programme II. We also thank M. Kappler, T. Kurtz, M. Neuhofer, O. Sachs, and R. Sporn for providing in situ pictures of the meteorite finds. The samples for analyses were donated by Lukas Smula, Ralph Sporn, and Martin Neuhofer. This is greatly acknowledged.

Appendix A. Supplementary data

Supplementary material related to this article can be found, in the online version, at doi:https://doi.org/10.1016/j.chemer.2019.07.007.

References

Barnes, J.J., Goodrich, C.A., McCubbin, F.M., Bischoff, A., Decker, S., Boyce, J.W., 2019. Non-chondritic volatile signatures in a ureilite trachyandesite (abstract #1875). 50th Lunar and Planetary Science Conference.

Barrat, J.-A., Zanda, B., Moynier, F., Bollinger, C., Liorzou, C., Bayron, G., 2012. Geochemistry of CI chondrites: Major and trace elements, and Cu and Zn isotopes. Geochim. Cosmochim. Acta 83, 79–92.

Barrat, J.-A., Rouxel, O., Wang, K., Moynier, F., Yamaguchi, A., Bischoff, A., Langlade, J., 2015. Early stages of core segregation recorded by Fe isotopes in an asteroidal mantle. Earth Planet. Sci. Lett 419, 93–100.

Barrat, J.-A., Gillet, P., Dauphas, N., Bollinger, C., Etoubleau, J., Bischoff, A., Yamaguchi, A., 2016. Evidence from Tm anomalies for non-CI refractory lithophile element proportions in terrestrial planets and achondrites. Geochim. Cosmochim. Acta 176, 1–17.

Bartoschewitz, R., Appel, P., Barrat, J.-A., Bischoff, A., Caffee, M.W., Franchi, I.A., Gabelica, Z., Greenwood, R.C., Harir, M., Harries, D., Hochleitner, R., Hopp, J., Laubenstein, M., Mader, B., Marques, R., Morlok, A., Nolze, G., Prudêncio, M.I., Rochette, P., Ruf, A., Schmitt-Kopplin, Ph, Seemann, E., Szurgot, M., Tagle, R., Wach, R.A., Welten, K.C., Weyrauch, M., Wimmer, K., 2017. The Braunschweig meteorite – a recent L6 chondrite fall in Germany. Chemie der Erde – Geochemistry 77, 207–224.

Bhandari, N., Mathew, K.J., Rao, M.N., Herpers, U., Bremer, K., Vogt, S., Wölfli, W., Hofmann, H.J., Michel, R., Bodemann, R., Lange, H.-J., 1993. Depth and size dependence of cosmogenic nuclide production rates in stony meteoroids. Geochimica Cosmochimica Acta 57, 2361–2375.

Bhandari, N., Murty, S.V.S., Shukla, P.N., Shukla, A.D., Mahajan, R.R., Sarin, M.M., Srinivasan, G., Suthar, K.M., Sisodia, M.S., Jha, S., Bischoff, A., 2002. Itawa bhopji (L3-5) chondrite regolith breccia: fall, classification and cosmogenic records. Meteoritics & Planetary Science 37, 549–563.

Bhandari, N., Murty, S.V.S., Mahajan, R.R., Parthasarathy, G., Shukla, P.N., Sisodia, M.S., Rai, V.K., 2009. Kaprada L(5/6) chondrite: chemistry, petrography, noble gases and nuclear tracks. Planet. Space Sci. 57, 2048–2052.

Bischoff, A., Stöffler, D., 1992. Shock metamorphism as a fundamental process in the evolution of planetary bodies: information from meteorites. Europ. J. Mineral 4, 707–755.

Bischoff, A., Rubin, A.E., Keil, K., Stöffler, D., 1983. Lithification of gas-rich chondrite regolith breccias by grain boundary and localized shock melting. Earth Planet. Sci. Lett. 66, 1–10.

Bischoff, A., Geiger, T., Palme, H., Spettel, B., Schultz, L., Scherer, P., Schlüter, J., Lkhamsuren, J., 1993. Mineralogy, chemistry, and noble gas contents of adzhi-bogdo - an LL3-6 chondritic breccia with foreign clasts. Meteoritics 28, 570–578.

Bischoff, A., Scott, E.R.D., Metzler, K., Goodrich, C.A., 2006. Nature and origins of meteoritic breccias. Book chapter. In: Lauretta, D.S., McSween JrH.Y. (Eds.), Meteorites and the Early Solar System II. Univ. of Arizona, Tucson, pp. 679–712.

Bischoff, A., Horstmann, M., Pack, A., Laubenstein, M., Haberer, S., 2010. Asteroid 2008 TC_3 – almahata sitta: a spectacular breccia containing many different ureilitic and chondritic lithologies. Meteorit. Planet. Sci. 45, 1638–1656.

Bischoff, A., Jersek, M., Grau, T., Mirtic, B., Ott, U., Kučera, J., Horstmann, M., Laubenstein, M., Herrmann, S., Randa, Z., Weber, M., Heusser, G., 2011. Jesenice - a new meteorite fall from Slovenia. Meteorit. Planet. Sci. 46, 793–804.

Bischoff, A., Dyl, K.A., Horstmann, M., Ziegler, K., Wimmer, K., Young, E.D., 2013a. Reclassification of villalbeto de la peña – occurrence of a winonaite-related fragment in a hydrothermally metamorphosed polymict L-chondritic breccias. Meteorit. Planet. Sci. 48, 628–640.

Bischoff, A., Horstmann, M., Vollmer, C., Heitmann, U., Decker, S., 2013b. Chelyabinsk – not only another ordinary LL5 chondrite, but a spectacular chondrite breccia (abstract No. 5171). Meteorit. Planet. Sci. 48, A61.

Bischoff, A., Barrat, J.-A., Bauer, K., Burkhardt, C., Busemann, H., Ebert, S., Gonsior, M., Hakenmüller, J., Haloda, J., Harries, D., Heinlein, D., Hiesinger, H., Hochleitner, R., Hoffmann, V., Kaliwoda, M., Laubenstein, M., Maden, C., Meier, M.M.M., Morlok, A., Pack, A., Ruf, A., Schmitt-Kopplin, P., Schönbächler, M., Steele, R.C.J., Spurny, P., Wimmer, K., 2017a. The stubenberg meteorite - an LL6 chondrite fragmental breccia recovered soon after precise prediction of the strewn field. Meteorit. Planet. Sci. 52, 1683–1703.

Bischoff, A., Wurm, G., Chaussidon, M., Horstmann, M., Metzler, K., Weyrauch, M., Weinauer, J., 2017b. The allende multi-compound chondrule (ACC) – chondrule formation in a local super-dense region of the early solar system. Meteorit. Planet. Sci. 52, 906–924.

Bischoff, A., Schleiting, M., Wieler, R., Patzek, M., 2018. Brecciation among 2280 ordinary chondrites – constraints on the evolution of their parent bodies. Geochim. Cosmochim. Acta 238, 516–541.

Bischoff, A., Schleiting, M., Patzek, M., 2019. Shock stage distribution of 2280 ordinary chondrites – can bulk chondrites with a shock stage S6 exist as individual rocks? Meteorit. Planet. Sci. 54. https://doi.org/10.1111/maps.13208).

Burkhardt, C., Dauphas, N., Tang, H., Fischer-Gödde, M., Qin, L., Chen, J.H., Rout, S.S.,

Pack, A., Heck, P.H., Papanastassiou, D.A., 2017. In search of the earth-forming reservoir: mineralogical, chemical and isotopic characterizations of the ungrouped achondrite NWA 5363/5400 and selected chondrites. Meteorit. Planet. Sci. 52, 807–826.
Busemann, H., Baur, H., Wieler, R., 2000. Primordial noble gases in "phase Q" in carbonaceous and ordinary chondrites studied by closed-system stepped etching. Meteorit. Planet. Sci. 35, 949–973.
Consolmagno, G.J., Britt, D.T., Macke, R.J., 2008. The significance of meteorite density and porosity. Chemie der Erde 68, 1–29.
Cressy Jr, P.J., Bogard, D.D., 1976. On the calculation of cosmic ray exposure ages of stone meteorites. Geochim. Cosmochim. Acta 40, 749–762.
Crozaz, G., Pellas, P., Bourot-Denise, M., de Chazal, S.M., Fiéni, C., Lundberg, L.L., Zinner, E., 1989. Plutonium, uranium and rare earths in the phosphates of ordinary chondrites—The quest for a chronometer. Earth. Planet. Sci. Lett. 93, 157–169.
Di Gregorio, M., Busemann, H., Hunt, A.C., Krietsch, D., Schönbächler, M., Maden, C., 2019. Variable cosmogenic argon in L/LL5 chondrite knyahinya (abstract #6384). Meteorit. Planet. Sci. 54 #6384.
Ebert, S., Bischoff, A., 2016. the stubenberg (bavaria) ordinary chondrite breccia: the latest German meteorite fall. Meteorit. Planet. Sci. 51 Special Issue, #6137.
Eugster, O., Michel, T., Niedermann, S., Wang, D., Yi, W., 1993. The record of cosmogenic, radiogenic, fissiogenic, and trapped noble gases in recently recovered Chinese and other chondrites. Geochim. Cosmochim. Acta 57, 1115–1142.
Ferko, T.E., Schultz, L., Franke, L., Bogard, D.D., Garrison, D.H., Hutchison, R., Lipschutz, M.E., 2000. Exposure history of the mocs (L6) chondrite: a study of strewn field samples. Meteorit. Planet. Sci. 35, 1215–1227.
Freundel, M., Schultz, L., Reedy, R.C., 1986. Terrestrial ^{81}Kr-Kr ages of Antarctic meteorites. Geochim. Cosmochim. Acta 50, 2663–2673.
Gomes, C.B., Keil, K., 1980. Brazilian Stone Meteorites. University of New Mexico Press 161 pp.
Goodrich, C.A., Bischoff, A., O'Brien, D.P., 2014. Asteroid 2008 TC_3 and the fall of almahata sitta, a unique meteorite breccia. Elements 10, 31–37.
Haack, H., Farinella, P., Scott, E.R.D., Keil, K., 1996. Meteoritic, asteroidal, and theoretical constraints on the 500 Ma disruption of the L chondrite parent body. Icarus 119, 182–191.
Haack, H., Sørensen, A.N., Bischoff, A., Patzek, M., Barrat, J.-A., Midtskoge, S., Stempel, E., Laubenstein, M., Greenwood, R., Schmitt-Kopplin, P., Busemann, H., Maden, C., Bauer, K., Schönbächler, M., Dahl-Jensen, T., 2019. Ejby - a new H5/6 ordinary chondrite fall in copenhagen, Denmark. Meteorit. Planet. Sci. https://doi.org/10.1111/maps.13344.
Heber, V.S., Wieler, R., Baur, H., Olinger, C., Friedmann, T.A., Burnett, D.S., 2009. Noble gas composition of the solar wind as collected by the genesis mission. Geochim. Cosmochim. Acta 73, 7414–7432.
Hertkorn, N., Harir, M., Schmitt-Kopplin, Ph., 2015. Nontarget analysis of murchison soluble organic matter by high-field NMR spectroscopy and FTICR mass spectrometry. Magn. Reson. Chem. 53, 754–768.
Hertkorn, N., Harir, M., Cawley, K.M., Schmitt-Kopplin, Ph., Jaffé, R., 2016. Molecular characterization of dissolved organic matter from subtropical wetlands: a comparative study through the analysis of optical properties, NMR and FTICR/MS. Biogeosciences 13, 2257–2277.
Herwartz, D., Pack, A., Friedrichs, B., Bischoff, A., 2014. Identification of the giant impactor theia in lunar rocks. Science 344, 1146–1150.
Herzog, G.F., Caffee, M., 2014. Cosmic-ray exposure ages of meteorites. In Treatise on Geochemistry 2nd ed. In: In: Davies, A.M. (Ed.), Planets, Asteroids, Comets and The Solar System Vol. 2. Elsevier, pp. 419–453.
Heusser, G., Weber, M., Hakenmüller, J., Laubenstein, M., Lindner, M., Maneschg, W., Simgen, H., Stolzenburg, D., Strecker, H., 2015. GIOVE: a new detector setup for high sensitivity germanium spectroscopy at shallow depth. Eur. Phys. J. C75, 531.
Hochleitner, R., Kaliwoda, M., Günther, A., Schmidbauer, E., Hoffmann, V.H., Yamamoto, Y., Mikouchi, T., Heinlein, D., 2015. The new Bavarian meteorite machtenstein - a H5 ordinary chondrite found around 1956. Lunar Planet. Sci. Conference 46, 2453.
Horstmann, M., Bischoff, A., 2014. The almahata sitta polymict breccia and the late accretion of asteroid 2008 TC_3 - invited review. Chem. Erde 74, 149–184.
Horstmann, M., Bischoff, A., Pack, A., Laubenstein, M., 2010. Almahata sitta – fragment MS-CH: characterization of a new chondrite type. Meteorit. Planet. Sci. 45, 1657–1667.
Jenniskens, P., Rubin, A.E., Yin, Q.-Z., Sears, D.W.G., Sansdford, S.A., Zolensky, M.E., Krot, A.N., Blair, L., Kane, D., Utas, J., Verish, R., Friedrich, J.M., Wimpnny, J., Eppich, G.R., Ziegler, K., Verosub, K.L., Rowland, D.J., Albers, J., Gural, P.S., Grisby, B., Fries, M.D., Matson, R., Johnston, M., Silber, E., Brown, P., Yamakawa, A., Sanborn, M.E., Laubenstein, M., Welten, K.C., Nishiizumi, K., Meier, M.M.M., Busemann, H., Clay, P., MacAffee, M., Schmitt-Kopplin, Ph., Hertkorn, N., Glavin, D.P., Calahan, M.P., Dworkin, J.P., Wu, Q., Zare, R.N., Grady, M., Verchovsky, S., Emelyanenko, V., Naroenko, S., Clark, D., Girten, B., P.S. Worden. (the Novato Consortium), 2014. Fall, recovery and characterization of the novato L6 chondrite breccia. Meteorit. Planet. Sci. 49, 1–38.
Jochum, K.P., Willbold, M., Raczek, I., Stoll, B., Herwig, K., 2005. Chemical characterization of the USGS reference glasses GSA-1G, GSC-1G, GSD-1G, GSE-1G, BCR-2G, BHVO-2G and BIR-1G using EPMA, ID-TIMS, ID-ICP-MS and LA-ICP-MS. Geostand. Geoanal. Res. 29 (3), 285–302.
Kerraouch, I., Ebert, S., Patzek, M., Bischoff, A., Zolensky, M.E., Pack, A., Schmitt-Kopplin, P., Belhai, D., Bendaoud, A., Le, L., 2019. A light, chondritic xenolith in the murchison (CM) chondrite – formation by fluid-assisted percolation during metasomatism? Geochemistry - Chemie der Erde. https://doi.org/10.1016/j.chemer.2019.06.002.
Kieffer, S.W., 1975. From regolith to rock by shock. The Moon 13, 301–320.
Klemme, S., Prowatke, S., Münker, C., Magee, C., Lahaye, Y., Zack, T., Kasemann, S.A., Cabato, E.J.A., Kaeser, B., 2008. Synthesis and preliminary characterisation of new silicate, phosphate and titanite reference glasses. Geostand. Geoanal. Res. 32, 39–54.
Korochantseva, E.V., Trieloff, M., Lorenz, C.A., Buykin, A.I., Ivanova, M.A., Schwarz, W.H., Hopp, J., Jessberger, E.K., 2007. L-chondrite asteroid breakup tied to ordovician meteorite shower by multiple isochron Ar-40-Ar-39 dating. Meteorit. Planet. Sci. 42, 113–130.
Langenhorst, M.C., Iancu, V., Tarcea, N., Langenhorst, F., Popp, J., 2017. Raman spectroscopy of experimentally shocked oligoclase. Lunar Planet. Sci. Conf. 48 #1574.
Leya, I., Masarik, J., 2009. Cosmogenic nuclides in stony meteorites revisited. Meteorit. Planet. Sci. 44, 1061–1086.
Lodders, K., Fegley Jr, B., 1998. The Planetary Scientist`s Companion. Oxford University Press, New York, pp. 371.
Lorenzetti, S., Lin, Y., Wang, D., Eugster, O., 2003. Noble gases and mineralogy of meteorites from China and the Grove mountains, Antarctica: a 005 Ma cosmic ray exposure age of GRV 980040. Meteorit. Planet. Sci. 38, 1243–1253.
Meckenstock, R.U., von Netzer, F., Stumpp, C., Lueders, T., Himmelberg, A.M., Hertkorn, N., Schmitt-Kopplin, Ph., Harir, M., Hosein, R., Haque, S., Schulze-Makuch, D., 2014. Water droplets in oil are microhabitats for microbial life. Science 345 (6197), 673–676.
Marti, K., Graf, T., 1992. Cosmic-ray exposure history of ordinary chondrites. Annu. Rev. Earth Planet. Sci. 20, 221–243.
Metzler, K., Bischoff, A., Palme, H., Gellissen, M., 2010. Impact melt rocks from the L3-6 chondritic regolith breccia Northwest Africa (NWA) 869. 2010. Meteorit. Planet. Sci. 45, A137.
Metzler, K., Bischoff, A., Greenwood, R.C., Palme, H., Gellissen, M., Hopp, J., Franchi, I.A., Trieloff, M., 2011. The L3-6 chondritic regolith breccia Northwest Africa (NWA) 869: (I) petrology, chemistry, oxygen isotopes, and Ar-Ar age determinations. Meteorit. Planet. Sci. 46, 652–680.
Morlok, A., Bischoff, A., Patzek, M., Sohn, M., Hiesinger, H., 2017. Chelyabinsk – a rock with many different (stony) faces: an infrared study. Icarus 284, 431–442.
Niederer, F.R., Papanastassiou, D.A., Wasserburg, G.J., 1981. The isotopic composition of titanium in the allende and leoville meteorites. Geochim. Cosmochim. Acta 45, 1017–1031.
Pack, A., Herwartz, D., 2014. The triple oxygen isotope composition of the earth mantle and understanding $\Delta^{17}O$ variations in terrestrial rocks and minerals. Earth. Planet. Sci. Lett. 390, 138–145.
Pack, A., Tanaka, R., Hering, M., Sengupta, S., Peters, S., Nakamura, E., 2016. The oxygen isotope composition of San Carlos olivine on VSMOW2-SLAP2 scale. Rapid Commun. Mass Spectrom 30, 1495–1504.
Pack, A., Höweling, A., Hezel, D.C., Stefanak, M., Beck, A.K., Peters, S.T.M., Sengupta, S., Herwartz, D., Folco, L., 2017. Tracing the oxygen isotope composition of the upper earth atmosphere using cosmic spherules. Nat. Commun. 8, 15702.
Popova, O., Jenniskens, P., Emel'yanenko, V., Kartashova, A., Biryukov, E., Khaibrakhmanov, S., Shuvalov, V., Rybnov, Y., Dudorov, A., Grokhovsky, V.I., Badyukov, D.D., Yin, Q.Z., Gural, P.S., Albers, J., Granvik, M., Evers, L.G., Kuiper, J., Kharlamov, V., Solovyov, A., Rusakov, Y.S., Korotkiy, S., Serdyuk, I., Korochantsev, A.V., Larionov, M.Y., Glazachev, D., Mayer, A.E., Gisler, G., Gladkovsky, S.V., Wimpenny, J., Sanborn, M.E., Yamakawa, A., Verosub, K.L., Rowland, D.J., Roeske, S., Botto, N.W., Friedrich, J.M., Zolensky, M., Le, L., Ross, D., Ziegler, K., Nakamura, T., Ahn, I., Ik Lee, J., Zhou, Q., Li, X.H., Li, Q.L., Liu, Y., Tang, G.Q., Hiroi, T., Sears, D., Weinstein, I.A., Vokhmintsev, A.S., Ishchenko, A.V., Schmitt-Kopplin, Ph., Hertkorn, N., Nagao, K., Haba, M.K., Komatsu, M., Mikouchi, T., (The Chelyabinsk Airburst Consortium), 2013. Chelyabinsk airburst, damage assessment, meteorite recovery and characterization. Science 342, 1069–1073.
Qin, L., Alexander, C.M.O., Carlson, R.W., Horan, M.F., Yokoyama, T., 2010. Contributors to chromium isotope variation of meteorites. Geochim. Cosmochim. Acta 74, 1122–1145.
Riebe, M.E.I., Welten, K.C., Meier, M.M.M., Wieler, R., Barth, M.I.F., Ward, D., Laubenstein, M., Bischoff, A., Caffee, M.W., Nishiizumi, K., Busemann, H., 2017. Cosmic-ray exposure ages of six chondritic almahata sitta fragments. Meteorit. Planet. Sci. 52, 2353–2374.
Righter, K., Abell, P., Agresti, D., Berger, E.L., Burton, A.S., Delaney, J.S., Fries, M.D., Gibson, E.K., Haba, M.K., Harrington, R., Herzog, G.F., Keller, L.P., Locke, D., Lindsay, F.N., McCoy, T.J., Morris, R.V., Nagao, K., Nakamura-Messenger, K., Niles, P.B., Nyquist, L.E., Park, J., Peng, Z.X., Shih, C.-Y., Simon, J.I., Swisher, I.I.I.C.C., Tappa, M.J., Turrin, B.D., Zeigler, R.A., 2015. Mineralogy, petrology, chronology, and exposure history of the Chelyabinsk meteorite and parent body. Meteorit. Planet. Sci. 50, 1790–1819.
Rubin, A.E., 1990. Kamacite and olivine in ordinary chondrites: intergroup and intragroup relationships. Geochim. Cosmochim. Acta 54, 1217–1232.
Rubin, A.E., Moore, W.B., 2011. What´s up? Preservation of gravitational direction in the larkman nunatak 06299 LL impact melt breccia. Meteorit. Planet. Sci. 46, 737–747.
Ruf, A., Kanawati, B., Hertkorn, N., Yin, Q.Z., Moritz, F., Harir, M., Lucio, M., Michalke, B., Wimpenny, J., Shilobreeva, S., Bronsky, B., Saraykin, V., Gabelica, Z., Gougeon, R., Quirico, E., Ralew, S., Jakubowski, T., Haack, H., Jenniskens, P., Hinman, N.W., Schmitt-Kopplin, Ph., 2017. Previously unknown class of metalorganic compounds revealed in meteorites. Proc. Nat. Acad. Sci. 114, 2819–2824.
Salisbury, J.W., 1993. Mid-infrared spectroscopy: laboratory data. In: Pieters, C.M., Englert, P.A.J. (Eds.), Remote Geochemical Analysis: Elemental and Mineralogical Composition. Cambridge University Press.
Salisbury, J.W., D'Aria, D.M., 1989. Measurement of christiansen frequencies in spectra of particulate samples for determination of rock composition. Lunar Plant. Sci. Conf. 20 #940.
Salisbury, J.W., D'Aria, D.M., Jarosewich, E., 1991. Midinfrared (2.5-13.5 μm) reflectance spectra of powdered stony meteorites. Icarus 92, 280–297.
Schmitt-Kopplin, Ph., Gabelica, Z., Gougeon, R.D., Fekete, A., Kanawati, B., Harir, M.,

Gebefuegi, I., Eckel, G., Hertkorn, N., 2010. High molecular diversity of extraterrestrial organic matter in murchison meteorite revealed 40 years after its fall. PNAS 107 (7), 2763–2768.
Schmitt-Kopplin, Ph., Harir, M., Kanawati, B., Tziotis, D., Hertkorn, N., Gabelica, Z., 2012. Chemical footprint of the solvent soluble extraterrestrial organic matter occluded in sołtmany ordinary chondrite. Meteorite J. 1–2, 79–92 Special issue Soltmany.
Schönbächler, M., Rehkämper, M., Lee, D.-C., Halliday, A.N., 2004. Ion exchange chromatography and high precision isotopic measurements of zirconium by MC-ICP-MS. Analyst 129, 32–37.
Sears, D.W., Grossman, J.N., Melcher, C.L., Ross, L.M., Mills, A.A., 1980. Measuring metamorphic history of unequilibrated ordinary chondrites. Nature 287, 791–795.
Shields, W.R., Murphy, T.J., Catanzaro, E.J., Garner, E.L., 1966. Absolute isotopic abundance ratios and the atomic weight of a reference sample of potassium. J. Res. Nat. Bur. Stand. Sect. A: Phys. Chem. 70A, 193–197.
Spurný, P., 2016. Instrumentally documented meteorite falls: two recent cases and statistics from all falls. In: Chesley, S., Morbidelli, A., Jedicke, R., Farnocchia, D. (Eds.), Asteroids: New Observations, New Models. Proceedings IAU Symposium No. 318, pp. 69–79.
Spurný, P., Borovička, J., Shrbený, L., 2007. Automation of the Czech part of the European fireball network: equipment, methods and first results. In: Milani, A., Valsecchi, G.B., Vokrouhlický, D. (Eds.), Near Earth Objects, Our Celestial Neighbors: Opportunity and Risk, pp. 121–130 IAU Symposium 236.
Spurný, P., Borovicka, J., Haloda, J., Shrbeny, L., Heinlein, D., 2016. Two very precisely instrumentally documented meteorite falls: Žďár nad sázavou and stubenberg – prediction and reality. Meteorit. Planet. Sci. 51 Special Issue, # 6221.
Spurný, P., Borovička, J., Baumgarten, G., Haack, H., Heinlein, D., Sørensen, A.N., 2017a. Atmospheric trajectory and heliocentric orbit of the Ejby meteorite fall in Denmark on February 6, 2016. Planet. Space Sci. 143, 192–198.
Spurný, P., Borovička, J., Mucke, H., Svoreň, J., 2017b. Discovery of a new branch of the taurid meteoroid stream as a real source of potentially hazardous bodies. Astronomy & Astrophysics 605 id.A68, 25 pp.
Steele, R.C.J., Schönbächler, M., 2016. High precision mass-independent Cr isotope compositions by MC-ICPMS and MC-TIMS: application to terrestrial and meteorite samples. Goldschmidt abstract #2947.
Stöffler, D., Keil, K., Scott, E.R.D., 1991. Shock metamorphism of ordinary chondrites. Geochim. Cosmochim. Acta 55, 3845–3867.
Storz, J., Bischoff, A., Degering, D., Ebert, S., Heinlein, D., Jull, T., Kontul, I., Li, X., Merchel, S., Oberst, J., Ott, U., Pack, A., Peters, S., Petö, M.K., Rugel, G., 2017. Cloppenburg (H4-5) - First Results of a New Find. abstract #0075. URL:. Paneth Kolloquium, Nördlingen (Germany). http://www.paneth.eu/PanethKolloquium/2017/0075.pdf.
The Meteoritical Bulletin, https://www.lpi.usra.edu/meteor/about.php.
Theulé, P., Duvernay, F., Danger, G., Borget, F., Bossa, J.B., Vinogradoff, V., et al., 2013. Thermal reactions in interstellar ice: a step towards molecular complexity in the interstellar medium. Adv. Space Res. 52 (8), 1567–1579.
Trinquier, A., Birck, J.L., Allègre, C.J., Göpel, C., Ulfbeck, D., 2008a. ^{53}Mn–^{53}Cr systematics of the early solar system revisited. Geochim. Cosmochim. Acta 72, 5146–5163.
Trinquier, A., Birck, J.-L., Allègre, C.J., 2008b. High-precision analysis of chromium isotopes in terrestrial and meteorite samples by thermal ionization mass spectrometry. J. Anal. At. Spectrom. 23, 1565–1574.
Trinquier, A., Elliott, T., Ulfbeck, D., Coath, C., Krot, A.N., Bizzarro, M., 2009. Origin of nucleosynthetic isotope heterogeneity in the solar protoplanetary disk. Science 324, 374–376.
Tziotis, D., Hertkorn, N., Schmitt-Kopplin, Ph., 2011. Kendrick-analogous network visualisation of ion cyclotron resonance fourier transform (FTICR) mass spectra: improved options to assign elemental compositions and to classify organic molecular complexity. Eur. J. Mass Spectrom. 17, 415–421.
Ward, D., Bischoff, A., Roszjar, J., Berndt, J., Whitehouse, M.J., 2017. Trace element inventory of meteoritic Ca-phosphates. Am. Mineral. 102, 1856–1880.
Wasson, J.T., Kallemeyn, G.W., 1988. Compositions of Chondrites. Philosophical Transactions of the Royal Society of London. Series A, Mathematical and Physical Sciences: 325, No. 1587. The Solar System: Chemistry as a Key to Its Origin, pp. 535–544.
Weisberg, M.K., McCoy, T.J., Krot, A.N., 2006. Systematics and evaluation of meteorite classification. Book chapter. In: Lauretta, D.S., McSween JrH.Y. (Eds.), Meteorites and the Early Solar System II. Univ. of Arizona, Tucson, pp. 19–52.
Weyrauch, M., Bischoff, A., 2012. Macrochondrules in chondrites – formation by melting of mega-sized dust aggregates and/or by rapid collisions at high temperatures? Meteorit. Planet. Sci. 47, 2237–2250.
Wieler, R., 2002. Cosmic-ray-produced noble gases in meteorites. Rev. Mineral. Geochem 47, 125–170.
Williams, N.H., 2015. The Origin of Titanium Isotopic Anomalies Within Solar System Material. PHD Thesis. The University of Manchester.
Zeng, X., Li, S., Leya, I., Wang, S., Smith, T., Li, Y., Wang, P., 2018. The kumtag 016 L5 strewn field, xinjiang Province, China. Meteorit. Planet. Sci 53, 1113–1130.
Zhang, J., Dauphas, N., Davis, A.M., Pourmand, A., 2011. A new method for MC-ICPMS measurement of Ti isotopic composition: identification of correlated isotope anomalies in meteorites. J. Anal. At. Spectrom. 26, 2197–2205.
Zhang, J., Dauphas, N., Davis, A.M., Leya, I., Fedkin, A., 2012. The proto-earth as a significant source of lunar material. Nat. Geosci. 5, 251–255.
Zolensky, M.E., Ivanov, A., 2003. The kaidun microbreccia meteorite: a harvest from the inner and outer asteroid belt. Chem. Erde 63, 185–246.
Zolensky, M.E., Ivanov, A.V., Yang, S.V., Mittlefehldt, D.W., Ohsumi, K., 1996. The kaidun meteorite: mineralogy of an unusual CM1 lithology. Meteorit. Planet. Sci. 31, 484–493.
Zolensky, M., Herrin, J., Mikouchi, T., Ohsumi, K., Friedrich, J., Steele, A., Rumble, D., Fries, M., Sandford, S., Milam, S., Hagiya, K., Takeda, H., Satake, W., Kurihara, T., Colbert, M., Hanna, R., Maisano, J., Ketcham, R., Goodrich, C.A., Le, L., Robinson, G., Martinez, J., Ross, K., Jenniskens, P., Shaddad, M.H., 2010. Mineralogy and petrography of the almahata sitta ureilite. Meteorit. Planet. Sci. 45, 1618–1637.